National Library of Canada

Acquisitions and Bibliographic Services Branch

395 Wellington Street
Ottawa, Ontario
K1A 0N4

Bibliothèque nationale du Canada

Direction des acquisitions et des services bibliographiques

395, rue Wellington
Ottawa (Ontario)
K1A 0N4

NOTICE

The quality of this microform is heavily dependent upon the quality of the original thesis submitted for microfilming. Every effort has been made to ensure the highest quality of reproduction possible.

If pages are missing, contact the university which granted the degree.

Some pages may have indistinct print especially if the original pages were typed with a poor typewriter ribbon or if the university sent us an inferior photocopy.

Reproduction in full or in part of this microform is governed by the Canadian Copyright Act, R.S.C. 1970, c. C-30, and subsequent amendments.

AVIS

La qualité de cette microforme dépend grandement de la qualité de la thèse soumise au microfilmage. Nous avons tout fait pour assurer une qualité supérieure de reproduction.

S'il manque des pages, veuillez communiquer avec l'université qui a conféré le grade.

La qualité d'impression de certaines pages peut laisser à désirer, surtout si les pages originales ont été dactylographiées à l'aide d'un ruban usé ou si l'université nous a fait parvenir une photocopie de qualité inférieure.

La reproduction, même partielle, de cette microforme est soumise à la Loi canadienne sur le droit d'auteur, SRC 1970, c. C-30, et ses amendements subséquents.

Canadä

UNIVERSITY OF ALBERTA

FABRICATION OF SUPERCONDUCTOR-INSULATOR-SUPERCONDUCTOR TUNNEL JUNCTIONS

BY

© MICHAEL WALTER KONEVECKI

A THESIS
SUBMITTED TO THE FACULTY OF GRADUATE STUDIES AND RESEARCH IN PARTIAL FULFILLMENT FOR THE DEGREE OF MASTER OF SCIENCE

DEPARTMENT OF ELECTRICAL ENGINEERING

EDMONTON, ALBERTA
FALL 1993

National Library of Canada

Bibliothèque nationale du Canada

Acquisitions and Bibliographic Services Branch

Direction des acquisitions et des services bibliographiques

395 Wellington Street
Ottawa, Ontario
K1A 0N4

395, rue Wellington
Ottawa (Ontario)
K1A 0N4

The author has granted an irrevocable non-exclusive licence allowing the National Library of Canada to reproduce, loan, distribute or sell copies of his/her thesis by any means and in any form or format, making this thesis available to interested persons.

L'auteur a accordé une licence irrévocable et non exclusive permettant à la Bibliothèque nationale du Canada de reproduire, prêter, distribuer ou vendre des copies de sa thèse de quelque manière et sous quelque forme que ce soit pour mettre des exemplaires de cette thèse à la disposition des personnes intéressées.

The author retains ownership of the copyright in his/her thesis. Neither the thesis nor substantial extracts from it may be printed or otherwise reproduced without his/her permission.

L'auteur conserve la propriété du droit d'auteur qui protège sa thèse. Ni la thèse ni des extraits substantiels de celle-ci ne doivent être imprimés ou autrement reproduits sans son autorisation.

ISBN 0-315-88037-6

Canada

UNIVERSITY OF ALBERTA

RELEASE FORM

NAME OF AUTHOR: **Michael W. Konevecki**

TITLE OF THESIS: **Fabrication of Superconductor-Insulator-Superconductor Tunnel Junctions**

DEGREE: **Master of Science**

YEAR THIS DEGREE GRANTED: **1993**

Permission is hereby granted to the University of Alberta Library to reproduce single copies of this thesis and to lend or sell such copies for private, scholarly or scientific research purposes only.

The author reserves all other publication and other rights in association with the copyright in the thesis, and except as herein before provided neither the thesis nor any substantial portion thereof may be printed or otherwise reproduced in any material form whatever without the author's prior written permission.

Michael W. Konevecki

Michael W. Konevecki
#201, 10422-78 Ave.
Edmonton, Alberta
Canada T3B 3B6

Dated: August 12, 1993

UNIVERSITY OF ALBERTA

FACULTY OF GRADUATE STUDIES AND RESEARCH

The undersigned certify that they have read, and recommend to the Faculty of Graduate studies and Research for acceptance, a thesis entitled **Fabrication of Superconductor-Insulator-Superconductor Tunnel Junctions** submitted by **Michael Konevecki** in partial fulfillment of the requirements for the degree of **Master of Science.**

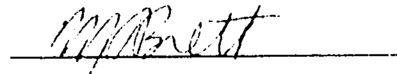

Dr. M.J. Brett - Supervisor

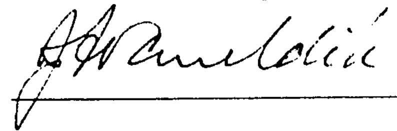

Dr. J. F. Vaneldik

Dr. A.C. Pierre

Date May 14, 1993

Abstract

This thesis describes the fabrication and testing of niobium and niobium nitride superconductor-insulator-superconductor (SIS) edge-geometry junctions. NbN and Nb SIS edge junctions with MgO tunneling barriers were deposited by planar magnetron sputtering techniques. The edges where tunneling occurs were formed by one of two methods; reactive ion etching and ion milling. NbN edge junctions produced by dc reactive sputtering were not successfully fabricated using reactive ion-etching. Nb edge junctions with very high critical current densities of 20 kA/cm^2 and junction areas of 0.5 (μm)^2 were produced using a reactive ion etch (RIE) edge definition process. However, these junctions showed a large leakage current greater than 50 μA (for some junctions, this is up to one-quarter of the knee current). Use of a 3 cm argon ion gun to ion mill a tunneling edge also produced junctions with excessive leakage. Various techniques were attempted to reduce this leakage, including reactively sputtering MgO in an oxygen rich ambient to ensure proper insulator stoichiometry, and exposing the tunneling barrier to a dc oxygen plasma to oxidize any pinholes.

Acknowledgments

I am deeply indebted to the two research assistants it has been my good fortune to have had the opportunity to work with. I was introduced to the science of thin films under Ken Westra's patient tutelage. Dr. Kevin Kornelson's enthusiasm for processing and keen use of experiments was a very positive example to follow. Bruce Veidt's strong interest in using SIS junctions in a receiver provided impetus in trying to provide a finished product. My supervisor, Dr. Michael Brett, provided a secure, steady foundation for my work. This thesis would not have been possible without the strong support of the Alberta Microelectronic Centre, both financially and by providing excellent facilities and expertise. I would like to mention several AMC employees foremost in my thoughts; Graham McKinnon, Glen Fitzpatrick, Alan Mitchell, Doug Bowles, and Yan Loke. Thank you all.

Table Of Contents

1 **Introduction**

1.1 Motivation 1

1.2 Superconductor-Insulator-Superconductor (SIS) junctions 1

1.2.1 Characteristics of real SIS junctions 7

1.3 Previous work 7

1.4 Other applications of junctions 11

2 **Mask design and Photoresist Processing**

2.1 Lithography and Processing 12

2.2 Mask design 14

2.3 Thin film deposition techniques 19

2.3.1 DC and RF Magnetron sputtering 19

2.3.2 Thermal and e-beam evaporation 22

2.4 Reactive Ion Etching (RIE) 23

3 **NbN/MgO/NbN Edge Junction Fabrication**

3.1 Reactive sputtering and optimization of NbN 28

3.2 NbN SIS device fabrication 33

3.3 NbN SIS Device Results 40

4 Nb/MgO/Nb Edge junction Fabrication

4.1 Nb Fabrication 42

4.1.1 Photoresist lift-off 47

4.1.2 RIE etch process 48

4.1.3 Ion beam milling Nb 48

4.2 Summary of Nb SIS Junction Fabrication Experiments 50

4.3 DC Nb/MgO/Nb Test results 53

4.4 Discussion of Test Results 58

5 Conclusion

5.1 Summary 62

5.2 Suggestions for Future work 64

References 65

Appendix A Optical properties of NbN. 69

List Of Tables

Table

4.0 Nb/MgO/Nb SIS junction fabrication experiments 52

4.1 Nb edge junction characteristics 54

List of Figures

Figure

1-1 Semiconductor analogy of an SIS junction 3

1-2 Ideal SIS I-V characteristic 5

1-3 Edge junction schematic 8

2-1, 2-2, 2-3 Photolithography mask set 16,17,18

2-4 Schematic of sputtering system 21

2-5 Schematic of Reactive Ion etcher 25

2-6 a,b RIE etch rates of Nb and NbN 26,27

3-1 NbN voltage versus N_2 sputtering hysteresis curve 29

3-2 NbN T_C measurements 31

3-3 NbN edge junction fabrication process 34-35

3-4 SEM photo of lift-off problem 36

3-5 Photo of completed die 38

3-6 Photo of junction area 39

3-7 NbN/MgO/NbN dc I-V characteristic 41

4-1-4.2 Nb edge junction fabrication processes 43-46

4-3 SEM photo of Nb/SiO edge 49

4-4 a,b DC I-V curves of Batch #5 and 6 Nb/MgO/Nb edge junctions 55

4-5 MgO thickness vs. deposition time 57

4-6a, 4-6b Batch #8a effect of O_2 plasma on Nb/MgO/Nb junctions 59

4-7 Critical current vs. sputtering time for unoxidized junctions 60

List of Symbols

ξ	Superconducting coherence length
Δ	Superconducting energy gap
I_c	Junction Critical current
R_N	Normal state resistance
R_S	Subgap resistance
h	Planck's constant
J_c	Josephson critical current
Jc	SIS junction critical current
sccm	standard (0° C, 1 Atmosphere) cubic centimeters per minute
ω	radial frequency of light
f	frequency in Hz
e	electronic charge 1.6×10^{-19} C

Chapter 1

Introduction

1.1 Motivation

The motivation for this research was the need for small area superconductor-insulator-superconductor (SIS) junctions for heterodyne receivers by the James Clerk Maxwell Telescope (JCMT) group, whose instrument is operating on Mauna Kea in Hawaii. This thesis reports on research concerning small area edge-geometry SIS junctions, in an attempt to satisfy receiver requirements. Alongside the development of edge junctions, a research associate (with the part-time assistance of a technician from the Electrical Engineering department at the University of Alberta) is developing planar tunnel junctions. While the fabrication techniques differ considerably, these two efforts are mutually supporting in terms of the materials studied and optimized, and in sharing and maintaining the large assortment of equipment needed for fabrication. With both edge and planar processes, the aim is to produce small area, high-speed (low-capacitance) junctions capable of working at 345 GHz. A particular attraction of the edge process is the ease of producing submicron area junctions. Using this process, it is possible to produce a junction of nominal area 0.5 $(\mu m)^2$ with a minimum planar feature size of 5 μm. In comparison, the constraints of our photolithographic equipment limit our planar process to approximately 1 $(\mu m)^2$.

1.2 Superconductor-Insulator-Superconductor (SIS) junctions

Recently developed processing techniques and materials are opening up new possibilities for radio astronomers observing at millimeter and submillimeter wavelengths. Many molecules in star-forming regions of interstellar space have sharp rotational transitions in the millimeter and submillimeter wavelength bands. The line strength, frequency and width of these molecular emissions can be used to calculate the relative density and velocity of interstellar matter, which can be used to infer

regions of new star birth in very distant galaxies as well as our own galaxy. Atmospheric attenuation at these frequencies is very heavy, however, due to absorption by water vapor and other molecules, and until recently there were few telescopes dedicated to operating in the mm and submm portion of the electromagnetic spectrum. In addition, fundamental difficulties arise in the fabrication of telescopes, receivers and detectors which work at these short wavelengths. Another challenge for astronomers at these wavelengths is the relatively low emission strength. Recently however, large expenditures have been made on several new telescopes including the Swedish-ESO (15 m diameter dish), the Caltech submillimeter observatory (10.4 m) and the James Clerk Maxwell telescope (JCMT 15 m). The latter two are situated at 4200 m above sea level on Mauna Kea in Hawaii, where water vapor absorption is minimal and the air is usually stable.

Until about 12 years ago, heterodyne receivers in the millimeter band used a Schottky diode as the non-linear mixing element. (A good reference for millimeter diode receivers is given in [1]). However, several drawbacks make working with semiconductor based diodes undesirable. The local oscillator power requirement is large ($\sim 10^{-4}$ W), which is difficult to produce at the frequencies involved [2]. The non-linearity in the I-V characteristic of a cooled Schottky diode occurs above 10 mV, which is much larger than the voltage scale of the incoming photon energy, $\hbar\omega/e$. This results in more noise. In addition, Schottky diode receivers have conversion loss.

In 1978, J. Tucker developed a quantum mechanical theory of microwave mixing using new superconductor-based elements, which offered a very promising alternative to Schottky diodes[3]. These new devices were superconductor-insulator-superconductor (SIS) junctions. An SIS junction consists of a thin insulator sandwiched between two superconductors. For very thin insulators (on the order of 1-2 nm), the electron wavefunctions of the two superconductors overlap, and quantum mechanical tunneling results. The very sharp non-linearity in the I-V characteristic of SIS junctions results from the unique density of states in superconductors. Figure 1-1

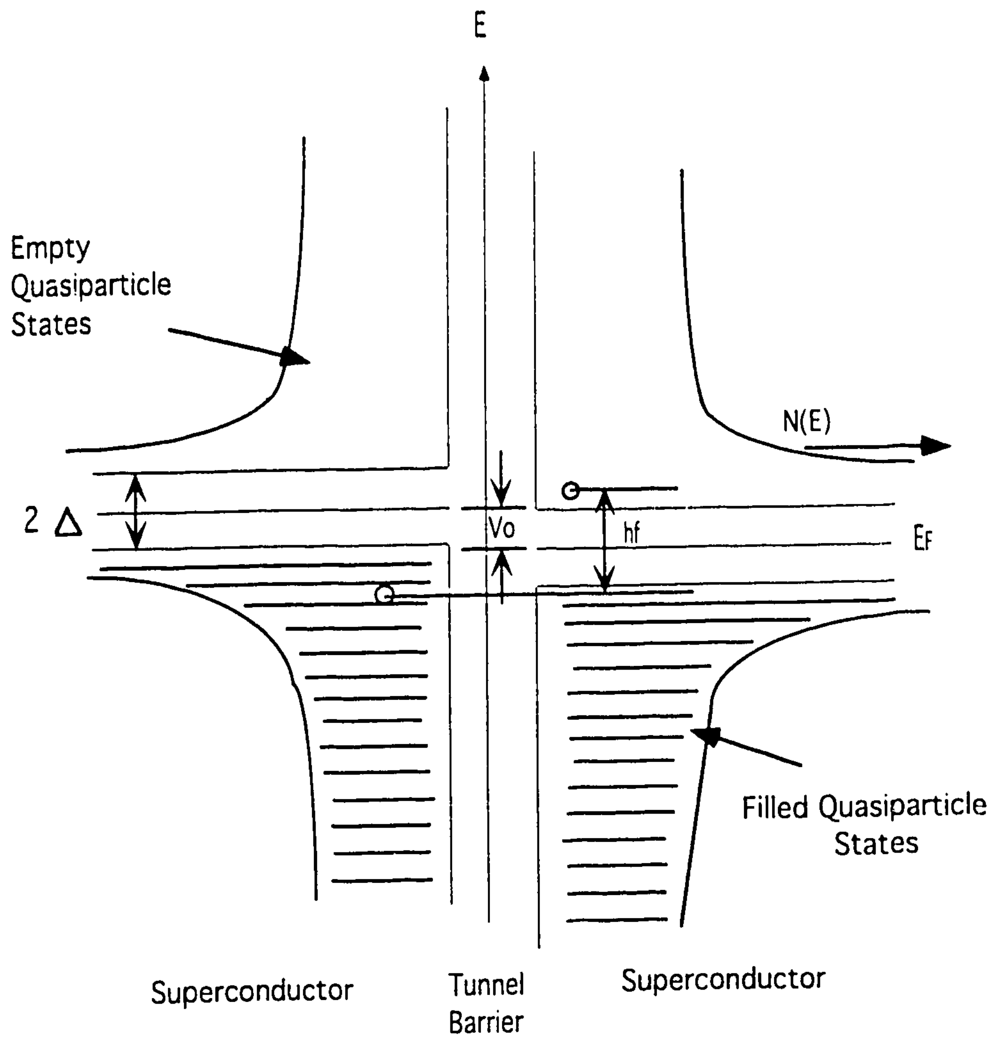

Figure 1-1 The semiconductor analogy of an SIS junction showing photon assisted tunneling of a quasiparticle.

shows what is often referred to as the semiconductor picture of an SIS junction. A large non-linearity in the density of states occurs at the bottom of the energy gap. The sharpness of the non-linearity can be less than a fraction of a millivolt, which is less than the equivalent voltage of the photon-assisted tunneling quasiparticle. The result is that the noise temperature level of this mixer can be very much reduced and can theoretically approach the quantum limit. By applying the signal to be measured together with the appropriate local oscillator to the junction (non-linear mixing), the resulting down-converted output can theoretically have conversion gain if the receiver is specially constructed. This greatly reduces the noise temperature contribution of subsequent IF amplifiers. However, conversion gain only occurs with very careful matching. In practice, most practical receivers do not have conversion gain so that they are more stable and operate over a wider bandwidth.

Superconductivity arises as the result of the small attractive force between pairs of electrons known as Cooper pairs [4]. The value of the energy gap is Δ, therefore the minimum energy needed to break a Cooper pair is 2Δ. An important parameter of a superconductor is its coherence length, ξ, which is the spatial extent of the Cooper pair. The size of discontinuities in the crystal lattice such as grain boundaries and non-stoichiometric material relative to the coherence length determine how close the actual energy gap of the material approaches the theoretical limit at a given temperature. Electrons excited across the gap have a finite lifetime and are distinguished by referring to them as "quasiparticles". Analogous to semiconductors, the quasiparticles can be excited across the gap thermally or assisted by absorbed photons. In figure 1-1, there is a bias voltage, V_0, across the junction. An electron is seen crossing the gap by acquiring an energy hf and tunneling through the barrier. This is referred to as photon assisted tunneling and gives rise to steps in the I-V characteristic of voltage width hf/e. The I-V characteristic of an ideal SIS junction at a temperature of 0 K is shown in figure 1-2. No tunneling occurs until the filled ground state of one superconductor overlaps the empty "conduction" band of the other. The

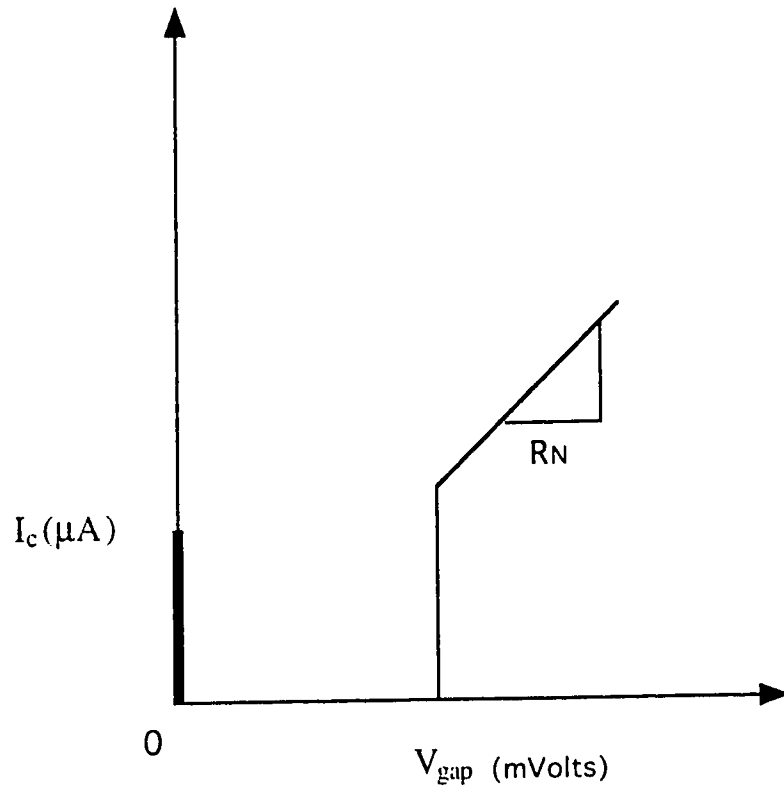

Figure 1-2 Ideal SIS I-V characteristic at 0 Kelvin.

increase in current at this point is abrupt because of the singularity in the density of states. Beyond this voltage the superconductor surpasses its critical current density and becomes a normal conductor, although tunneling still occurs above the gap voltage. The slope in the I-V characteristic at this point is R_n, the normal state resistance.

In summary, real SIS receivers have the following advantages: lower noise temperatures are obtainable, local oscillator power requirements are small ($\sim 10^{-9}$ W) and conversion gain is possible.

Some confusion exists between SIS and Josephson junctions. The junctions are physically similar, but the Josephson effect relies on the tunneling of Cooper pairs between the superconductors while the SIS junction in this application is associated with the so-called quasiparticle current resulting from the tunneling of broken Cooper pairs [5]. The Josephson effect may be suppressed by the presence of a strong magnetic field in the vicinity of the junction.

The first SIS junctions were made of lead and have been used successfully for about a decade in radio telescopes. The initial popularity of lead resulted from its long coherence length, and the ease with which it may be oxidized to form a tunneling barrier. The current trend has been away from lead and its alloys, for several reasons. Lead is a soft material, and when cycling the junction from 4.2 K to room temperature stress induced "hillocking" results which eventually destroys the junction. Lead alloys have smaller gap energies, 2Δ , and therefore are restricted to lower frequencies.

For these reasons, a more robust, mechanically stable material with a higher critical temperature, T_c, is desired. Niobium and NbN are hard refractory materials, which are chemically stable and are more suitable for thermal cycling. While the T_c of Nb is near 9.2 K, for NbN the T_c is around 16 K and the gap is near 5 mV. However, there are several disadvantages to working with niobium and its compounds, including having to physically deposit an insulator compatible and conformal with the base electrode, and the small superconducting coherence length, ξ, when working with NbN. In addition, there are three different oxides of niobium (including an insulator, a low T_c superconductor and a semiconductor) which can simultaneously exist, creating a poor

interface. Despite these drawbacks there is a large interest in Nb and NbN for use in SIS applications.

1.2.1. Characteristics of real SIS junctions

Real SIS junctions have several important differences from the idealized I-V characteristic of figure 1-2. A finite subgap resistance, R_{sg}, is caused by thermally assisted tunneling since the junctions are not at 0 K. Subgap leakage can also result through pinholes in the insulator. Broadening of the current non-linearity at the gap voltage occurs because there exist spatial non-uniformities in the superconducting material such as grain boundaries, impurities, varying thicknesses of the tunneling barrier and crystal defects near the barrier. Quantum mechanical effects are observable only when the voltage scale of the photon is comparable to the voltage width of the gap broadening. The gap voltage is the spatial average of all the local energy gaps across the interface [6]. When the size of these defects in the superconductor lattice is small compared to the coherence length, the gap will be reduced but will remain sharp. When these defects are large compared to the coherence length, gap reduction and smearing will result. Lastly, below a certain point in the gap voltage called the drop-back voltage, there is no stable non-zero voltage bias point. For proper mixer operation, the biasing must be above this point.

1.3 Previous work

NbN/MgO/NbN SIS edge-junctions have been successfully fabricated by Hunt et. al [7]. The distinguishing feature of the edge-geometry process is that the thickness of the base electrode is one of the dimensions of the junction. The other dimension is determined by the width of the counter-electrode, which is defined by standard optical lithography (See figure 1-3). A disadvantage of the edge-geometry is that this device is more sensitive to the materials properties and substrate induced

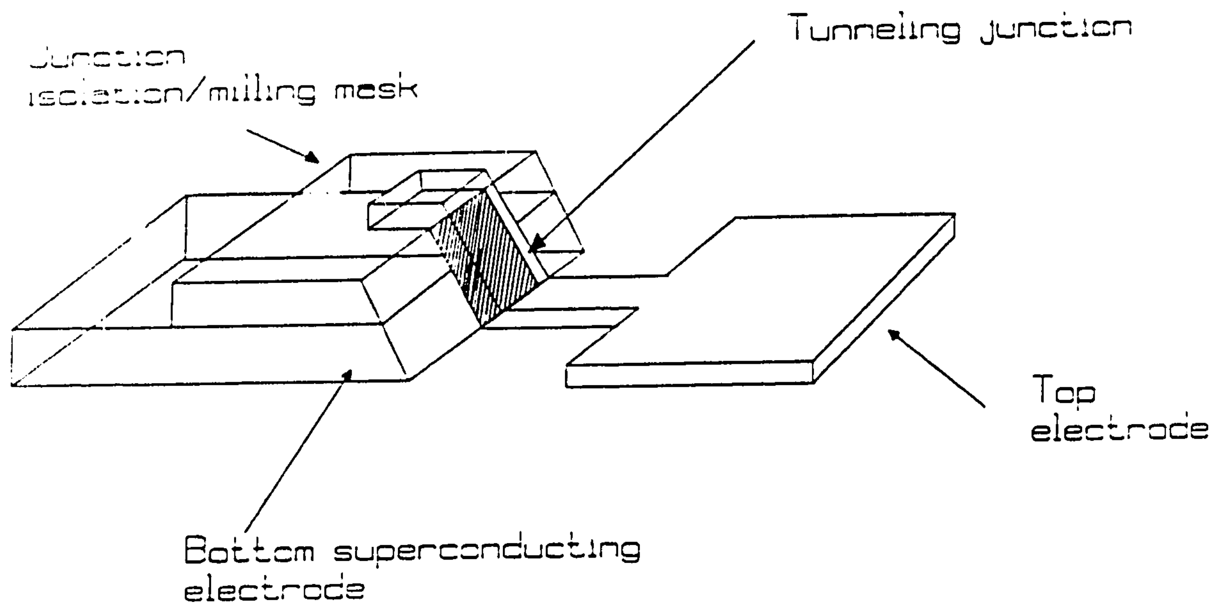

Figure 1-3 Schematic of edge junction geometry.

effects throughout the entire thickness of the film. One of the first documented applications of the edge junction fabrication process was given by Havermann to construct point contact metal-oxide-metal (MOM) diodes in 1978 [8]. This fabrication technique was later applied by many groups to reduce the area of SIS structure devices for use in radiotelescope receivers, for SQUIDs (Superconducting QUantum Interference Devices) and for fast logic circuits for use in Josephson supercomputers [9,10,11].

A wide variety of materials have been employed in the manufacture of SIS junctions. The choice of materials depends strongly on the design and/or performance requirements. Some of these considerations are; 1) critical temperature, T_c, which will determine the cost and reliability of the cryocooler required, 2) coherence length, which will determine the effect of film roughness on the sharpness of the I-V non-linearity, 3) choice of tunneling barriers, which will affect, among other things, junction capacitance and film stress, and finally 4) ease of depositing the barrier and controlling its stoichiometry and phase. One of the first materials used was Lead [12]. Lead is easily thermally evaporated, has a long coherence length, and forms its own high-quality oxide. Repeated thermal cycling between its low operating temperature of 4.2 K and room temperature usually destroys the junction by stress relaxation. Alloying Lead to decrease its stress usually reduces its gap voltage.

Somewhat later, refractory materials were considered for their mechanical and chemical stability. NbN was and is an important electrode material because it has a high critical temperature of 16 K and a large gap voltage (above 5 mV) which theoretically can allow it to operate above 1 THz [13, 14] . The T_c of NbN shifts downward when the composition varies from stoichiometric, and substrate heating is sometimes necessary to stabilize the high T_c B1 face-centered cubic crystal structure. NbN has a short coherence length, ξ, of 3-4 nm which requires a very smooth, abrupt interface between the superconductor and insulating barrier in order to obtain a sharp I-V characteristic. The insulating layer thickness must be less than 5 nm because of the small coherence length. The most common insulator used with NbN is MgO because

of its good lattice match (4% mismatch) and good chemical/electrical properties. However, the requirements of a smooth interface and a homogeneous insulator are difficult to accomplish in practice.

Currently, Nb is a popular material when used with Al/Al_2O_3 barriers [15]. Recent advances in two-stage closed cycle and hybrid cryocoolers, such as those available from RMC Cryosystems and others [16], capable of operating near liquid helium temperatures, have rendered the 9.2 K T_c of Nb acceptable. The coherence length of Nb is ten times longer than NbN, and Nb is much simpler to deposit repeatedly. Sputtered aluminum barriers which are later oxidized are the barriers of choice. Close control over the oxidation depth can be achieved by exposing a freshly sputtered Al layer to a pure oxygen atmosphere for a fixed length of time.

Edge junctions require a sloped superconducting edge which will be covered by the insulating barrier. Since proper formation of an tunneling edge is critical to the performance of these junctions, an introduction to fabrication processes follows. Sloped Nb or NbN profiles can be generated by reactive ion etching (RIE) with selected ratios of several etchant gases to erode the masking material at a faster rate than the electrode. One group masked their NbN with SiO_2 and obtained a sloped profile by controlling the percentage of CHF_3 added to pure CF_4 [17]. Another group etched an edge of an Nb film masked by photoresist by controlling the percentage of O_2 added to CF_4 [18]. Another method to generate a sloped etch profile is to simply tilt the substrates when etching them anisotropically. Advantages of using RIE to form a tunneling edge include quicker etch rates and less ion damage than from ion beam milling. However, one disadvantage is the possibility of leaving chemical residue on the edge from either the masking material or the etchant gases themselves.

The other common technique of forming a tunneling edge is by ion beam milling. This method consists of sputtering a sample using a stream of charged, inert atoms directed at the substrate at off-normal incidence. Since this is a purely physical removal method, no chemical residue is present. However, it has been found that for NbC_xN (NbN sputtered with some methane added to the discharge for high T_c

stabilization) based edge junctions, the junction quality is highly sensitive to the cutting and cleaning voltages used [19]. Also, when the tunneling barrier is formed by oxidizing the bottom electrode using a reactive ion beam (this consists of flowing one part of oxygen to two parts argon in the ion beam at much lower voltages than the edge cutting step) it has been found that it is crucial to keep the ion energy low to minimize damage and obtain high-gap, low-leakage junctions [20].

1.4 Other applictions of junctions

A wealth of new devices with SIS structures have been demonstrated that rely on their Josephson properties. A superconducting loop containing two Josephson junctions is the most sensitive detector for small changes in magnetic field strength. These devices are known as SQUIDs and are finding uses in magnetic resonance imaging in the medical field. Very precise voltage standards are possible using the a.c. Josephson effect because the junction voltage is a function of the frequency which can be very accurately controlled. By connecting large numbers of junctions in series it is possible to obtain a practical voltage standard of ten volts [21]. A large effort (principally by IBM in the early 1980's) was mounted to try to produce a Josephson supercomputer. The main attractions to Josephson logic elements are the very high switching speeds possible (on the order of picoseconds) and much smaller power dissipation levels compared to conventional semiconductor-based logic devices [22]. Successful demonstrations have been made but the effort has been stalled mainly by problems associated with fabrication process uniformity.

Chapter 2

Mask Design and Photoresist Processing

2.1 Lithography and Processing

Photolithography is essential to device fabrication since it provides the pattern transfer from a master mask to the wafer. The transferred pattern consists of a photosensitive, viscous polymer referred to as photoresist. The photoresist is applied onto a rotating substrate at low speed, during the spread cycle. After several seconds of spreading, the substrate is rapidly accelerated to several thousand rpm to promote a smooth continuous layer. A primer may be needed to promote adhesion between the photoresist and the substrate. Solvents in the photoresist are driven off using a vacuum hot plate or oven. Selected portions of the photoresist are exposed to UV light through a glass plate with an opaque pattern (usually a chrome film) preventing exposure in other areas. The substrate and mask are in close physical contact to reduce diffraction under the masking layer. The exposure to ultraviolet (UV) light increases the solubility of positive photoresist in developer, while negative resist has decreased solubility upon exposure. After developing, the photoresist is baked at high temperatures to toughen it and enable it to act as a mask, allowing etching (subtraction) from or film deposition (addition) onto the underlying substrate. The unexposed resist is then removed in another solvent.

Currently, new systems are being developed to expose photoresist using direct-write electron-beam guns or X-ray exposure sources. An e-beam can easily reproduce 0.1 μm planar scale features. E-beam systems are very slow and expensive, with high maintenance costs compared to conventional UV exposure sources. Therefore, for cheaply producing submicron scale junctions, the edge-geometry utilizing UV exposure is ideal.

The following list summarized the steps used for reliable transfer of 5 μm photoresist patterns:

1. Apply 1-2 ml of HPR-504 positive imaging photoresist onto the substrate during the two second spread cycle of 400 rpm.

2. Spin the substrate at 3500 rpm for 15 s to achieve approximately 1.4 μm thick photoresist.

3. Soft-bake the substrates at 110 °C for three minutes, then vacuum bake them for 50 s to drive off the solvent. Back-fill the bake chamber with dry nitrogen to vent to atmosphere.

4. Expose the photoresist to UV light for 8 seconds. The mask aligner used was a Quintel Q-404 utilizing a 365 nm UV filtered source and manual mask/wafer alignment.

5. Hand develop the unexposed photoresist in Shipley 354 NaOH based developer for ~15 s or in 352 for ~45 s.

6. Rinse the substrates thoroughly in deionized water and blow dry using a nitrogen gun.

7. For photoresist used as a dry or wet etch mask, hardbake for 3 minutes at 120 °C followed by a vacuum bake for two minutes. Vent with dry nitrogen.

8. For photoresist used as a lift-off mask, no hard bake is used. To remove the resist after the deposition, substrates are ultrasonically agitated in acetone.

2.2 Mask design

Three main processes were used to fabricate SIS edge junctions. The first masks for Process 1 are illustrated in figures 2-1 through 2-3. Mask 1 for Process 1 was photographically reversed in order to do photoresist lift-off processing in Process 2. In Process 3, a different isolation barrier was chosen for ion-milling. The original three mask set was designed using Generic Cadd 5.0 and fabricated by Shaw Photogrammetric in Nepean, Ontario. The masking material is a polymer known as emulsion which is cheaper than standard chrome but limits the smallest dimensions on the 4" X 4" masks to approximately 5 μm when photo-reduced 20 times. (Emulsion is also much softer than chrome and is more easily damaged during use and cleaning). The mask contains arrays of four die sites, each die containing pairs of junctions of one of four sizes. The junction sizes are 5, 10, 15 and 20 μm wide. The junction consists of two crossed lines which meet at right angles. The overlap of the edge of the bottom line with the top line defines the tunneling barrier.

The first mask (figure 2-1) defines the bottom electrode for junction contact. Two pads per device are required to allow four-point probe measurement of the junction resistance. Also on this mask are a series of test lines which may be observed using a scanning electron microscope to infer the geometry of the edges. The second mask (figure 2-2) defines the top superconducting electrode and may be displaced in the x and/or y directions by a much as 20 μm and still allow overlap of the two lines. This is an important consideration which greatly eases the restriction of mask registration for this step and is important during a many-step process where numerous opportunities exist for failure. To aid mask registration, along the edges of each of the die are sets of four-sided crosses which must be aligned to boxes on a subsequent or previous mask set. The individual die are ultimately separated by sawing through these alignment marks. The third mask shown in figure 2-3 exposes

clear areas above the bonding pads to allow chemical e.ching to contact the electrodes of these devices.

It was found that sharper profiles resulted in the junction isolation layer (produced by mask one) if this layer was lifted off rather than wet-etched. Wet etching tends to be an isotropic process proceeding in the vertical and horizontal directions at the same rate. This undercut can shadow the incoming MgO sputter flux causing shorts across the junction. (There is, however, a practical limit to the thickness of the film which can be lifted off leaving a vertical edge since the photoresist flows and leaves a sloped edge). To enable photoresist lift-off, a negative version of mask 1 had to be generated. This was generated by sputtering Nb on mask blanks and patterning them as if they were substrates.

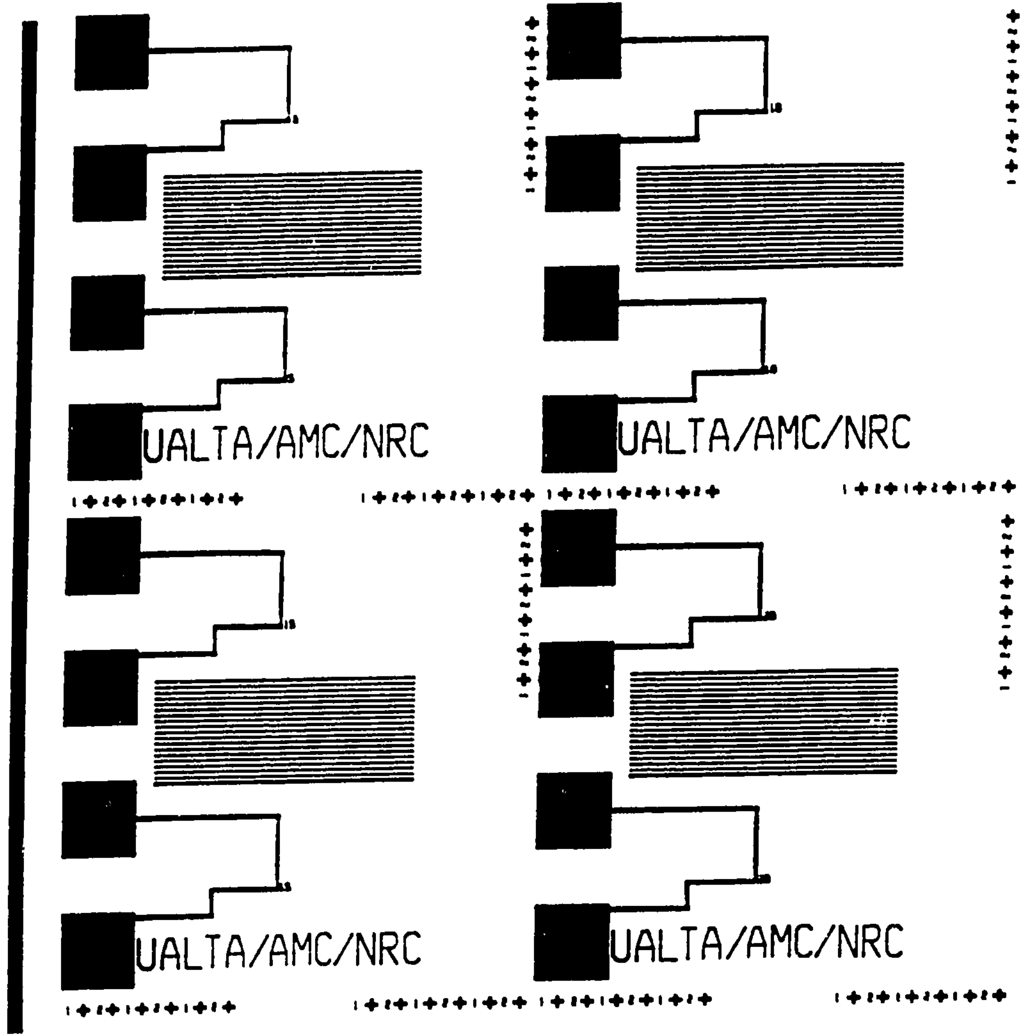

Figure 2-1 Mask 1: Bottom electrode / Tunneling edge mask.

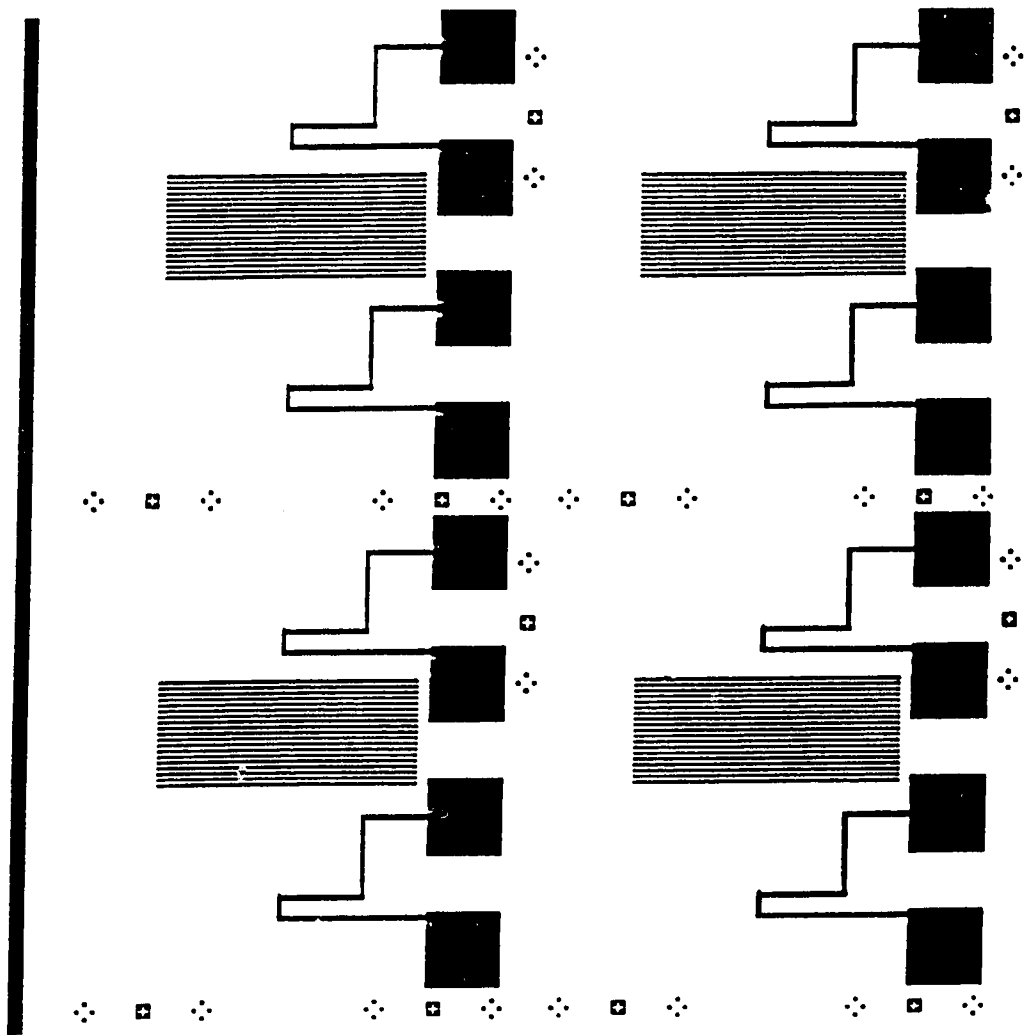

Figure 2-2 Mask 2: Top Electrode.

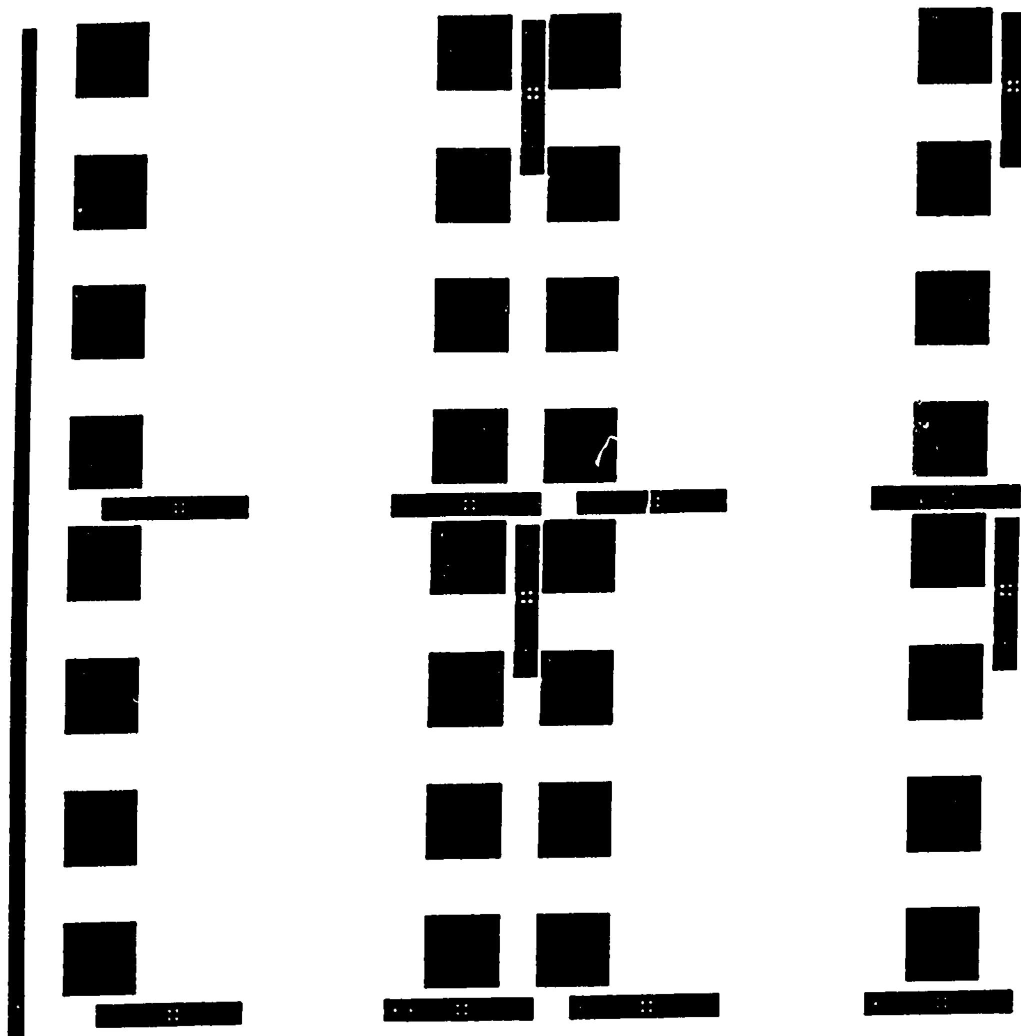

Figure 2-3 Mask 3 : Bonding pad etch windows.

2.3 Thin Film Deposition Techniques

Thin films are the basis of physical electronics, and controlling their properties is essential to controlling the devices they form. Thin films are deposited in vacuum chambers to avoid contamination of pure materials from atmospheric gases and to enhance growth rate. Many different techniques exist for depositing thin films including chemical vapor deposition (CVD), magnetron sputtering, rf sputtering and thermal and electron-beam evaporation. The two most important deposition methods used in this research were magnetron sputtering (dc and rf) and thermal and e-beam evaporation, discussed below.

2.3.1 DC and RF Magnetron Sputtering

Sputter deposition was used for all Nb, NbN and MgO layers of the devices. Sputtering is the ejection of atoms from a material caused by a momentum exchange with incoming particles [23]. The ejected flux may be accumulated on a substrate to form a thin film. The incoming particles are usually created in a low pressure plasma discharge. A wide range of materials may be sputtered since the incoming particle energy is usually much greater than the surface binding energies of most metals and compounds. Sputtering is done in a high vacuum system in order to reduce the contamination in the growing films and to increase the mean free path of the ejected material. During dc sputtering, the ionized (usually inert atoms) are accelerated into the target, which is held at a negative potential of several hundred volts. The plasma supplying ions for the sputtering process are maintained near the target surface by fixed magnets. These magnets increase the efficiency of ionization and thereby allow the plasma to be maintained at a lower pressure, as well as confine the plasma. If an insulating target is placed in a dc plasma, the positive ions would accumulate on the surface and extinguish the plasma immediately. The need to sputter insulators led to

the development of rf sputtering, where an rf generator is matched to the target. Over half of the cycle positive charges strike and accumulate on the target and during the other half electrons strike the surface and neutralize many of the ions.

Over the past decade sputtering has matured into a reliable film deposition process which is capable of depositing compounds of conducting and non-conducting materials. To deposit compounds, either a multi-element target may be employed or a reactive gas may be admitted into the chamber to form the desired material, though usually it is necessary to add a reactive gas to make up for a loss of material since sputtered compounds partially dissociate [24]. Neither method is trivial and some kind of compositional analysis is usually necessary to ensure the proper stoichiometry in the compound.

The sputtering system used in this study was from High Vacuum Systems (HVS) of Mississauga, Ontario. The chamber was a stainless steel box of dimensions 37"x20"x16". Two planar dc magnetrons accepted 5"x8" targets and an rf excited gun held 2" diameter circular targets. These were arranged on three sides of the chamber (See figure 2.4). The targets are shuttered to prevent cross-contamination. A rotatable carousel with shuttered facets could hold up to eight different substrates. An Ion-Tech 3 cm ion-gun was located in the lower chamber for ion-milling and edge cleaning. The pumping stack consisted of a Leybold Heraeus Trivac rotary pump and a CTI Cryo-Torr 8 cryogenic pump. Pressure measurement in the high vacuum range was done using an ion-gauge and a residual gas analyzer (RGA). Sputtering pressures were monitored using a capacitance manometer. Quicker pumpdowns were facilitated with 1.2 kW heater tape on the outside of the chamber to aid in removing water vapor adsorbed on the chamber walls. A base pressure of $4x10^{-7}$ Torr could routinely be achieved after about 30 hours of pumping.

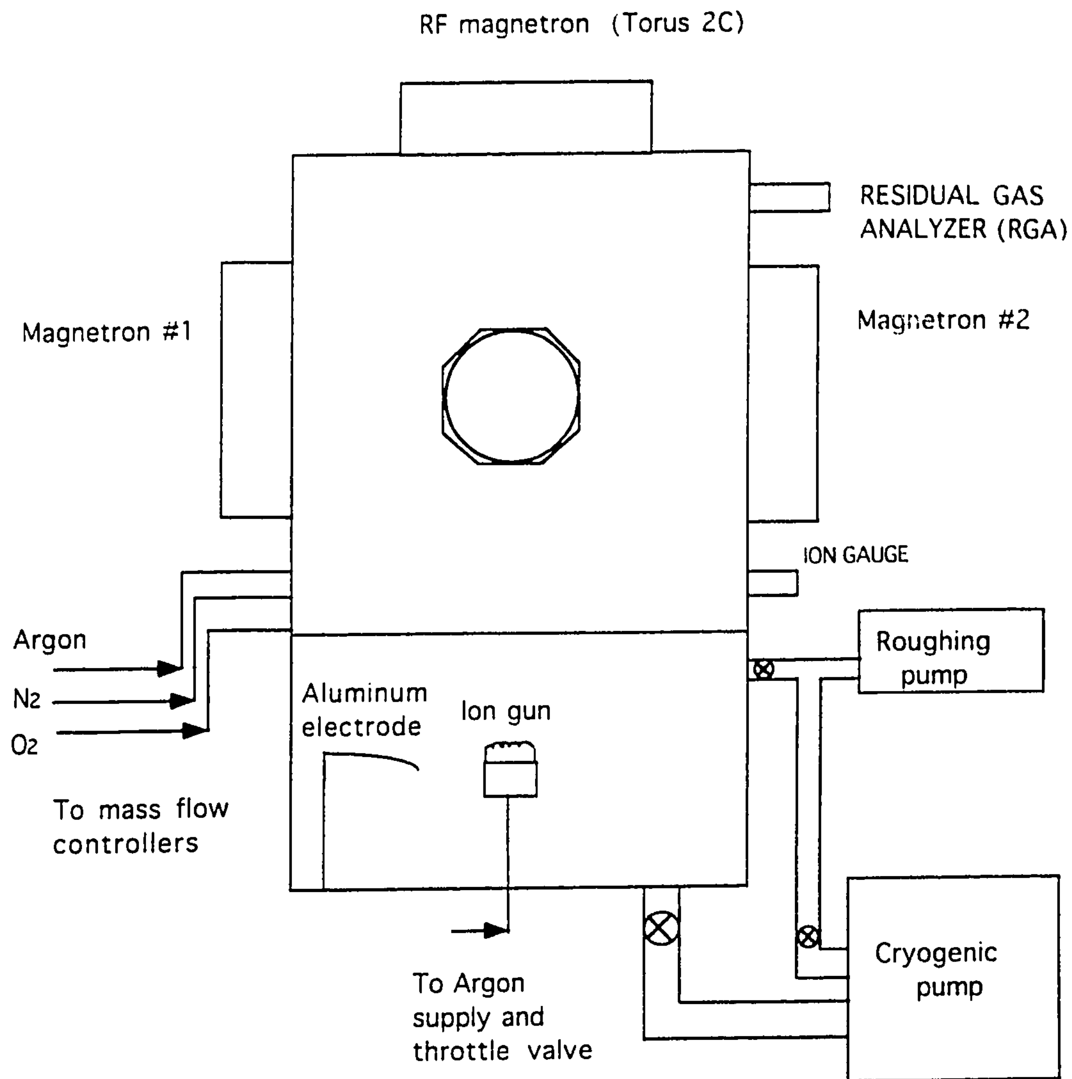

Figure 2-4 Schematic of the sputter system.

2.3.2 Thermal and E-beam Evaporation

Thermal evaporation of thin films was the first developed and simplest of film deposition techniques. The film material in the form of wire or pellets is placed into a "boat", a dish shaped strip of metal usually made of a refractory metal. The boat is resistively heated in an evacuated bell jar to evaporate the material inside it. Many variations of this technique exist including coating the inside of the boat to prevent contamination and forming the boat in the shape of a wire basket. The sources are constructed of refractory materials such as tungsten or tantalum because they have high melting points and low vapor pressures which minimize interactions with the melt. Some evaporant materials sublimate, explosively ejecting particles. For such materials, a baffled box, called a Drumheller source, ensures there is no line of sight path between the source and substrate preventing solid particles from reaching the substrate. Reactive evaporation is sometimes used with compounds which dissociate when heated.

Many desirable materials have a higher melting point than can be obtained conveniently by resistively heating a boat, and consequently suffer from contamination with the boat itself. For such materials, electron beam evaporation is ideal. In e-beam evaporation, an electron beam is rastered over a water-cooled crucible filled with the evaporant. This arrangement ensures the evaporant melts in its own environment and maintains good electrical grounding. In addition, much higher power densities can be achieved for use on low vapor pressure materials.

The thermal and e-beam evaporators used in this study were both rebuilt bell-jar systems from CHA Industries and have mechanical/diffusion pumping stacks. Base pressures in the mid to low 10^{-7} Torr range are routinely achieved after one and a half hours of pumping. The bell-jar on the thermal evaporator is water-cooled. An advantageous feature also available on the thermal system only is a planetary holder which rotates and revolves the substrates during deposition to improve film thickness

uniformity. Crystal thickness monitors are available on both systems. Boats with two different materials may be placed in the thermal evaporator (1 deposition at a time) while four different materials may be sequentially deposited in the e-beam system. Silicon monoxide (SiO) was deposited in the thermal evaporator from a Drumheller source to isolate the SIS junction and to passivate the entire chip. Alumina (Al_2O_3) was deposited in the e-beam system for use as a milling mask during ion-milling experiments.

2.4 Reactive Ion Etching

Reactive ion etching was one of the methods used for removing Nb and NbN to form a tunneling edge and for etching these materials away to form conducting lines. Reactive ion etching (RIE) is a dry anisotropic etching technique used to transfer small features in semiconductor device processing. An RIE consists essentially of a vacuum chamber with two parallel electrodes. The upper electrode is grounded and the bottom electrode, where the substrate sits, is powered by an rf generator connected through a matching network as in figure 2-5. The etchant gases are admitted into the chamber through flow meters. The rf generator creates a plasma in the chamber, typically between 10 and 100 mTorr. The differential mobilities of electrons and ions cause the plasma to acquire a positive charge relative to the grounded electrode. The etchant gas used was a mixture of CF_4 and O_2. Free fluorine atoms, dissociated in the plasma, are able to react with the film to be etched, forming volatile compounds which can be pumped away. Oxygen is usually added as a small fraction of the etchant gas (~5-10%) to prevent the build-up of non-volatile carbon-fluorine compounds by forming volatile CO_x compounds as well as freeing up fluorine. The term "reactive ion etching" is actually a misnomer as very few of the etchant species are actually ionized [25]. The electric field created by the plasma sheath accelerates charged ions into the substrate which enhances the anisotropy of the process. A good review of the various processes involved is given in Oehrlein [26]. Two techniques are commonly used to

determine when the etch is completed. One is simply to observe when a clear substrate with an opaque film clears (visual endpoint). The second technique is to observe the intensity of the optical emission lines from species of the etched film. Visual endpoint detection was used in this study. The RIE model used was a Plasma Therm Batchtop. This unit was calibrated for etch rates of Nb and NbN as a function of power and pressure as shown in figures 2-6 a and b.

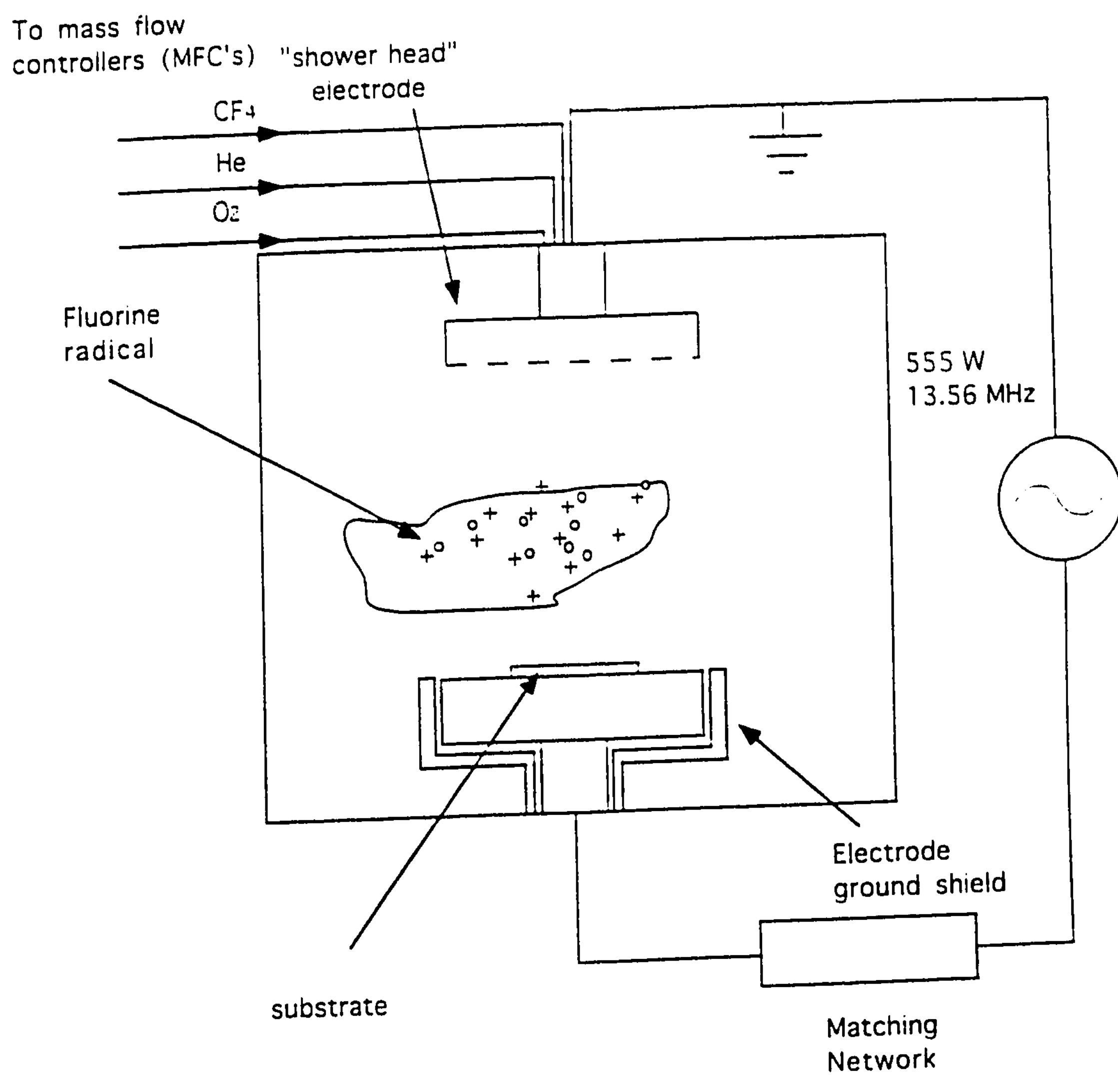

Figure 2-5 Schematic of the Reactive Ion Etcher (RIE) used.

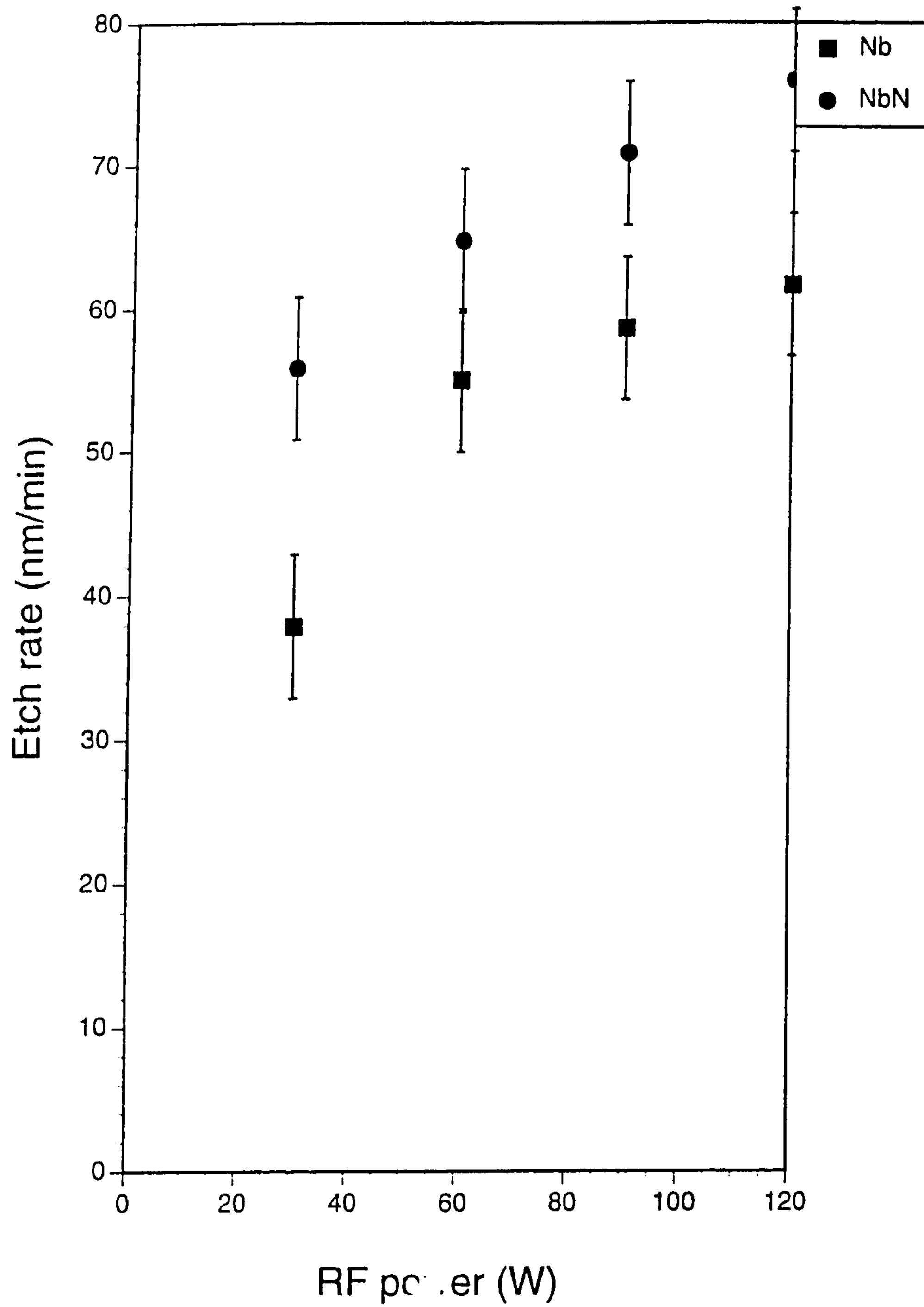

Figure 2-6 a Nb and NbN etch rates as a function of power with etch pressure fixed at 60 mTorr.

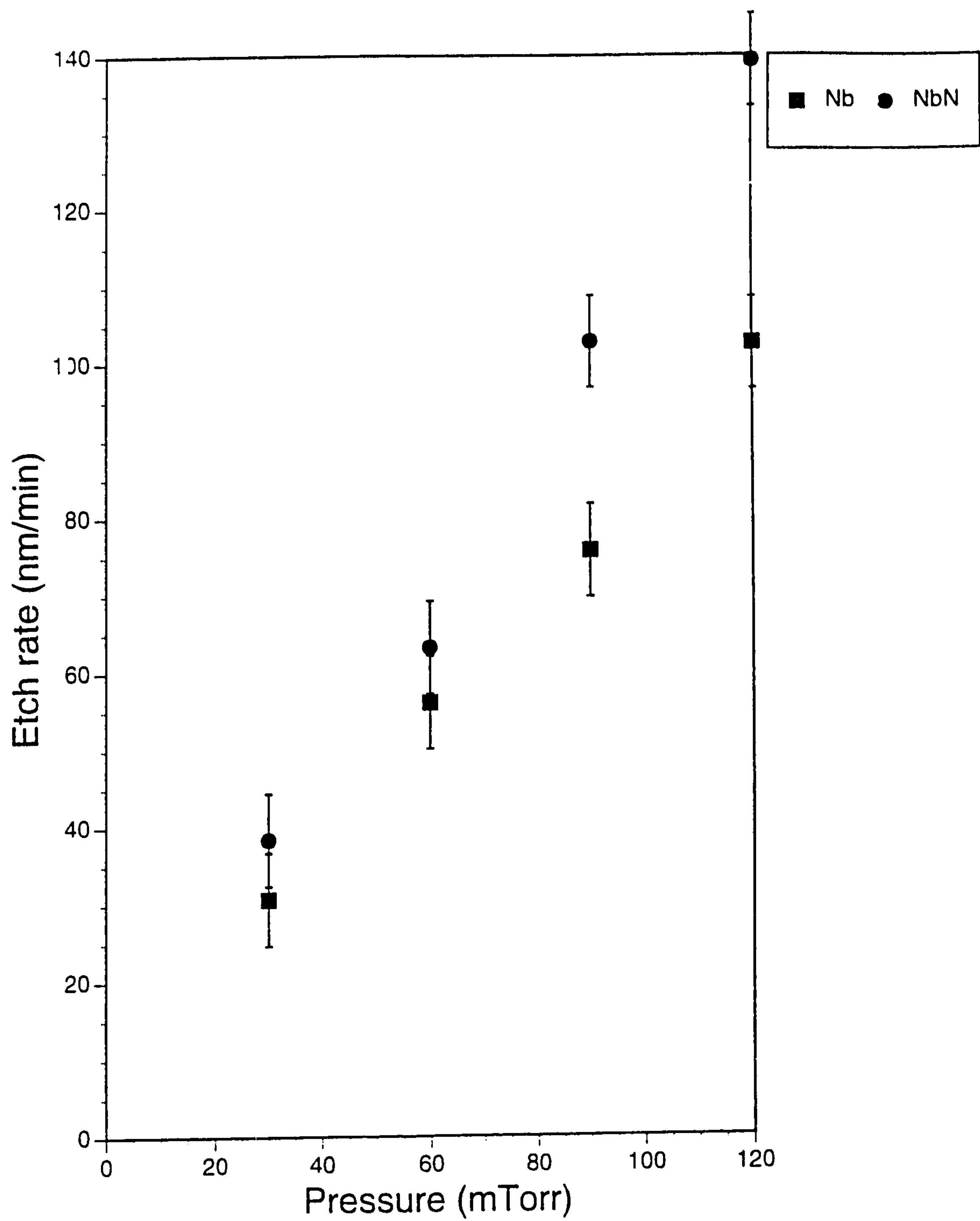

Figure 2-6 b Nb and NbN etch rates as a function of pressure with rf power fixed at 60 W (0.24 W/cm^2).

Chapter 3

NbN/MgO/NbN Edge Junction Fabrication

3.1 Reactive Sputtering and Optimization of NbN

The niobium nitride thin films used for edge junctions in this study were deposited by reactive dc sputtering. Reactive sputtering involves the addition of a reactive gas into the chamber during sputter deposition. This process is complicated by a hysteresis effect with the addition of the reactive gas during sputtering, as shown in figure 3-1 [27]. Optimization of reactively sputtered NbN is further complicated because the superconducting phase of NbN with B1 face-centered cubic crystal structure is metastable. The process used to reactively sputter relatively low stress films was as follows. Argon was admitted into the chamber and the pumping speed throttled to establish a pressure between 3 and 10 mTorr. Next, N_2 was turned on and increased, tracing out a voltage versus N_2 hysteresis curve. Films were deposited at various points on this curve. The film stress was inferred qualitatively from the bending of thin slices of microscope cover slides, measured with an optical microscope. The ends and center of this beam were focused on and the different distances noted. While this method is somewhat crude compared to measuring wafer bowing using laser interferometry, it is nonetheless possible to note trends. Magnetron sputtered films generally have compressive stress at low pressures with a transition to tensile stress at elevated pressures [28]. This transition was found to be near 7 mTorr argon pressure.

It was previously reported that the highest T_c films were deposited on the upper shoulder of the hysteresis curve [29]. A hysteresis curve similar to that in figure 3-1 was produced to find the optimum N_2 flow for the highest T_c film. Typically, what is seen is an increase in T_c near stoichiometric NbN followed by a decrease as the nitrogen flow is further decreased. The target voltage for each N_2 flow value was

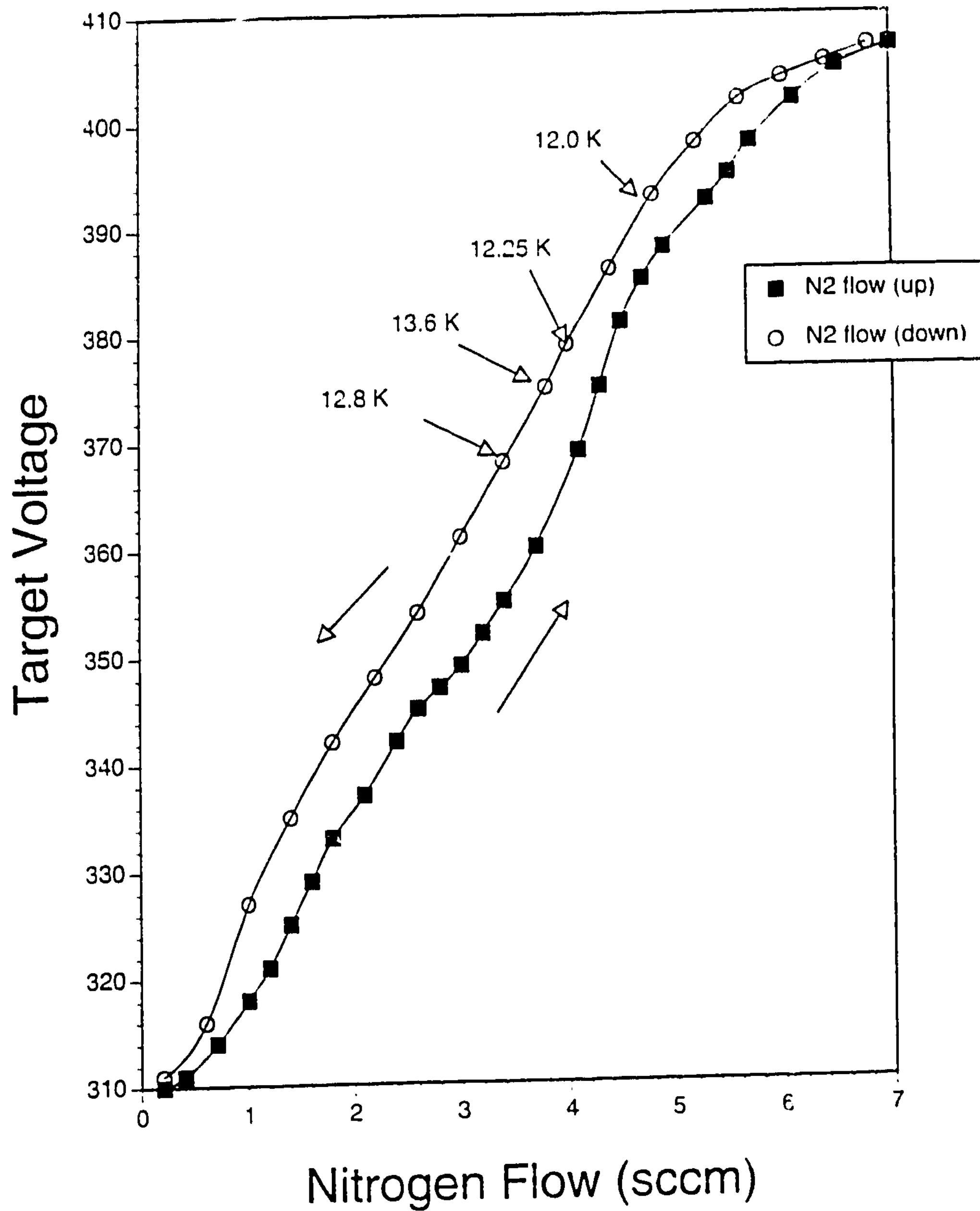

Figure 3-1 Hysteresis of target voltage with N_2 flow for NbN deposition. Two amps current, 5 mTorr pressure, and 40 sccm argon flow.

recorded, allowing the voltage to stabilize at each value of flow. The target voltage for a fixed flow is a sensitive indicator of the nitride content of the target surface and can be used to infer target nitridization. Typically, no more than five volts difference is observed from run to run. With heavy use of the target however, the erosion tracks deepen, intensifying the magnetic field created by permanent magnets behind the target. The ionization efficiency increases and the target voltage drops. For constant current (used to maintain nominally constant deposition rate) therefore, the target voltage will decrease over time, necessitating periodic recalibration of the hysteresis curve .

The characteristics of SIS junctions are critically dependent on the properties of the superconducting electrodes, in particular film stress and the superconducting critical temperature, T_c. Figure 3-2 is a plot of the NbN film resistance vs. temperature, which illustrates the dependence of T_c on stoichiometry. Increasing facet numbers coincide with decreasing N_2 flow. Prior to deposition the target was sputtered for 20 minutes in pure argon to remove any contamination or memory effects from previous depositions. The film T_c was measured in a cryostat containing a closed-cycle helium coldhead (CTI model 1020). A four-point probe was used to measure the resistance of the samples heat sunk to a large copper block using indium foil. Temperature measurement was performed using a calibrated commercially available silicon diode (Lake Shore DT 470). The definition of T_c used was the temperature at which the resistance drops to 50% of its value at 25 K. From this plot the highest T_c film was deposited at 4.8 sccm of N_2.

The argon sputter was optimized to minimize film stress. Excessive film stress may prevent films from adhering to their substrates. The stress was measured by observing the change in curvature of a microscope slide cover-slip before and after deposition. Films deposited below 5 mTorr exhibited tensile stress near 10^9 N/cm^2, estimated from substrate deformation. Based on these results, an argon pressure of 7 mTorr was chosen.

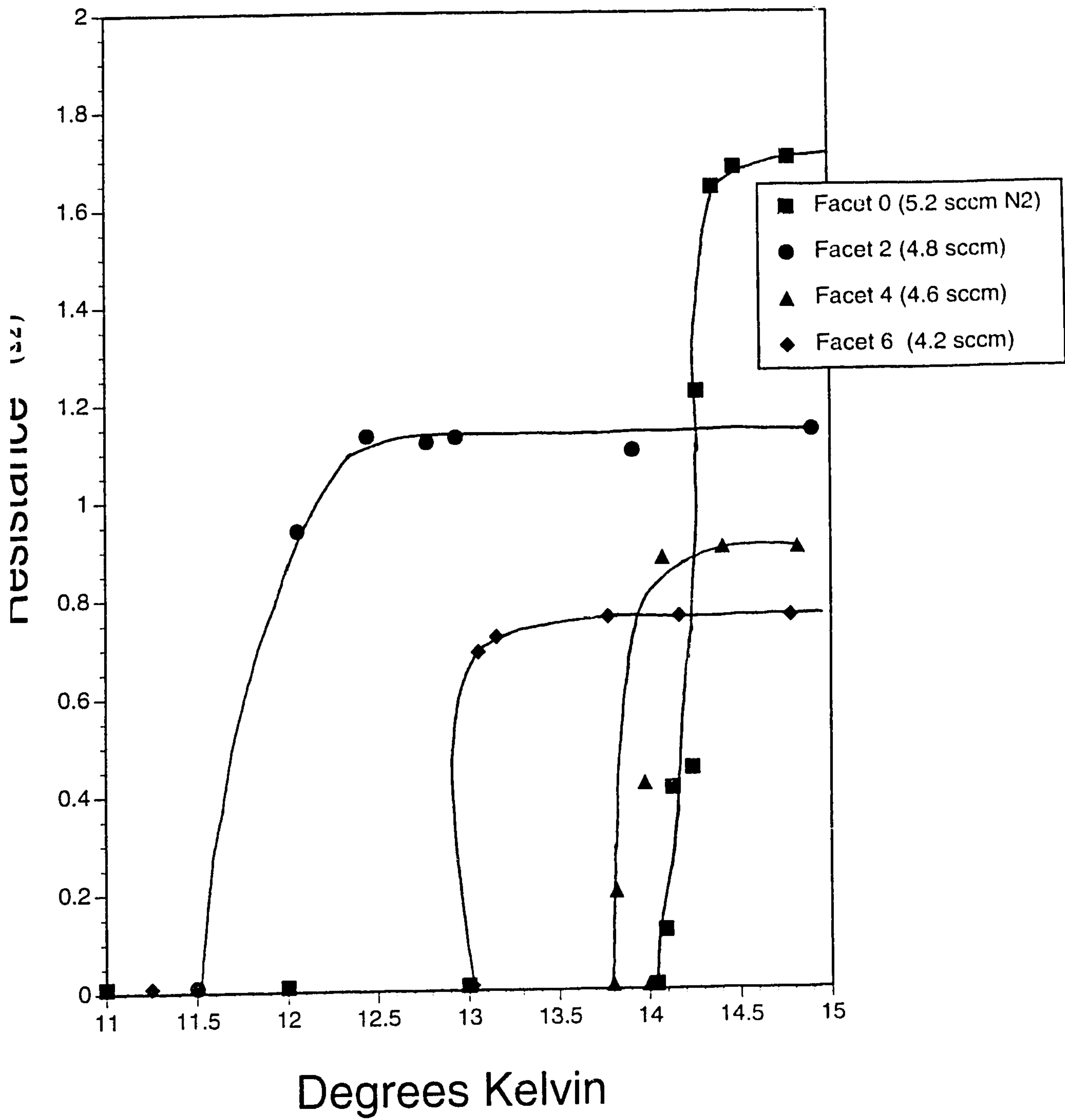

Figure 3-2 Resistance vs. Temperature plot for sputtered NbN films.

In addition to stress and critical temperature measurements, the optical properties of NbN were studied in order to further understand the quality of the reactively sputtered films. A spectroellipsometer was used to measure the pseudo-dielectric constant over the spectral interval 1.5 to 5.0 eV for four NbN films. A spectrophotometer was used to directly measure the film reflectivity, which confirmed the values calculated from the spectroellipsometer. The results of this study are in Appendix A.

3.2 NbN SIS Device Fabrication

Five separate NbN/MgO/NbN edge junction process runs were completed, numbered NbN1 to NbN5. Each process run took approximately ten days from initial substrate cleaning to helium dip testing, assuming all fabrication and testing equipment was working and available. Figure 3-3 outlines the steps used in fabrication. In process NbN1, MgO was used both to isolate the junction and to create the tunneling barrier. Wet etching the MgO in step 3 led to undercut which made covering the underlying edge with the tunneling barrier difficult in step 4. Junctions produced with this method (both Nb and NbN) most often proved to be shorts. In addition, the photoresist on the MgO was badly damaged during the etch and often appeared to end up on the substrate.

To eliminate undercut problems, photoresist lift-off of the initial NbN/MgO layer was used in Process NbN2. The photolithographic mask shown in Figure 2-1 was copied onto a blank 4"x4" mask plate and a negative copy was made. The sputtered NbN/MgO was grown in the photoresist well and then lifted-off. This eliminated wet-etching of the isolation mask, however the profile was still unsatisfactory since sputtered films are known to have decreasing density as the angle of incidence on the substrate increases [30]. This can lead to thinner and more voided films being deposited on the vertical edge. The end result was that the film profile was not sharp near the edge when the photoresist was removed, as revealed by a scanning electron microscope.

In the following run, NbN3, silicon monoxide was used to isolate the tunneling junction, replacing MgO in step 2. with sputtered MgO continuing as the barrier material in step 4. The SiO was thermally evaporated, with a planetary substrate holder to promote conformal coverage. Figure 3-4 is a scanning electron micrograph of an NbN/SiO edge with the SiO lifted off. The SiO film lifted off was far thicker than the sloped photoresist and this has produced an undesirable overhang above the edge. This overhang would prevent MgO sputter flux from uniformly covering the edge.

Figure 3.3 NbN Edge Junction Fabrication Process

1. Sputter NbN base layer.

2. MgO isolation layer sputtered and patterned with mask 1.

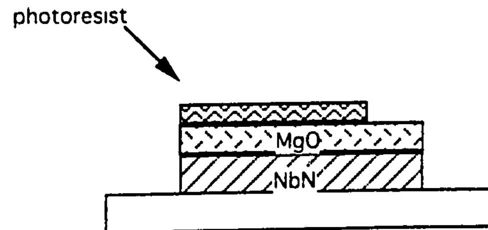

3. MgO wet etched in BOE. NbN etched in RIE.

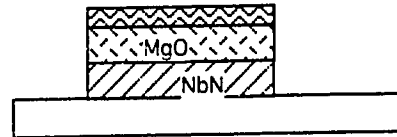

4. Remove photoresist. Rf sputter MgO tunneling barrier.

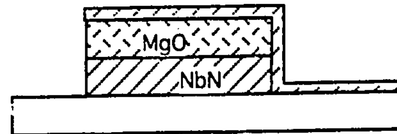

5. Deposit NbN counterelectrode.

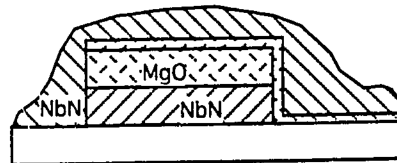

6. Pattern counterelectrode with mask 2 and plasma etch.

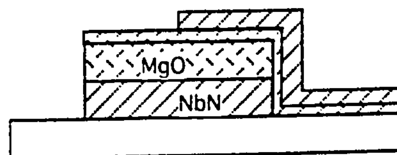

7. Deposit SiO passivation layer.

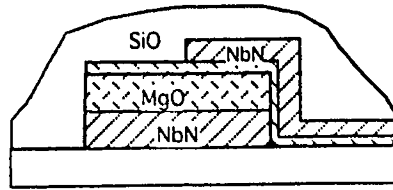

8. Pattern passivation layer with mask 3 and BOE etch through to bonding pads.

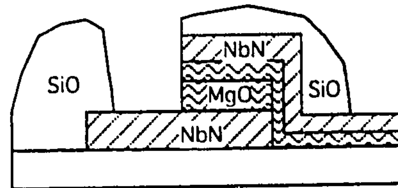

9. Dice wafer and test.

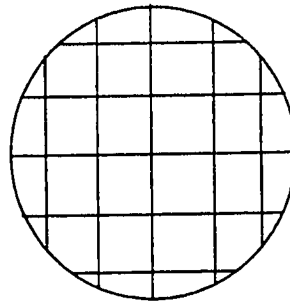

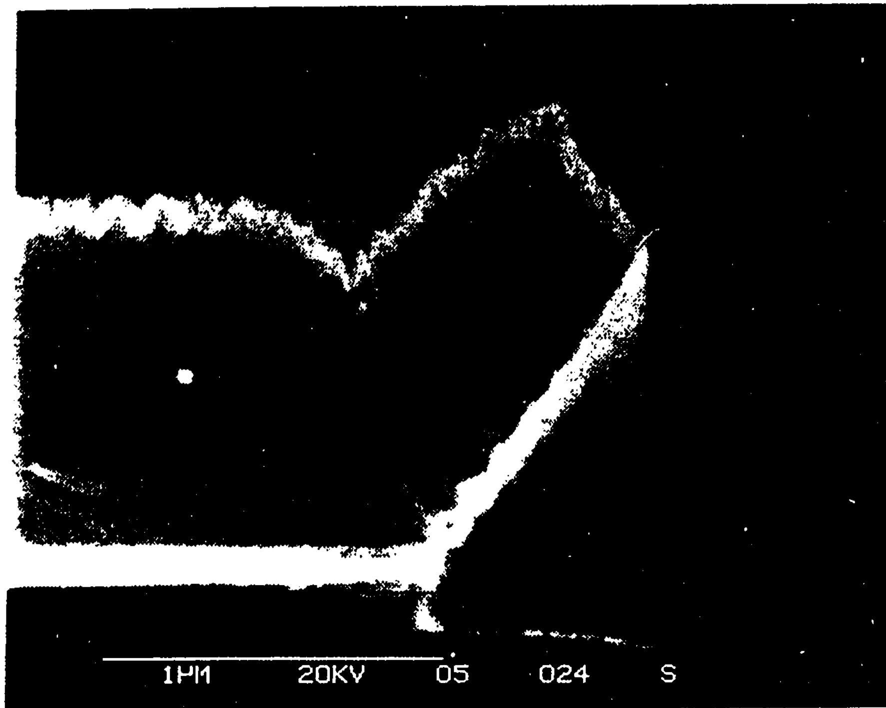

Figure 3-4 An SiO/NbN edge produced by RIE with the SiO layer lifted-off. The SiO layer was far too thick for proper lift-off. Note the film columnar structure perpendicular to the direction of the growth for the "ski-tip".

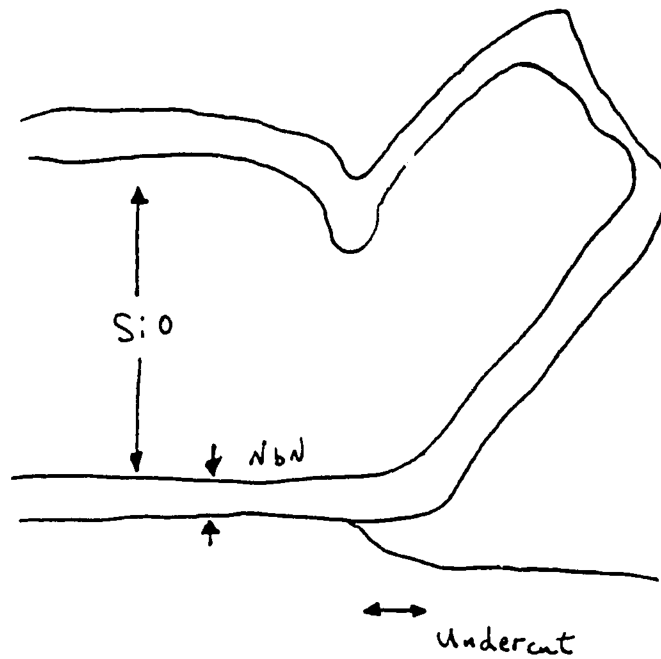

Much thinner lift-off films were later successfully used in NbN4. Using an evaporated SiO lift-off mask resulted in three large benefits. First, a good vertical isolation profile could be formed. Second, the SiO could be used as an etch mask, though it etches at approximately 1/3 the rate of NbN. Photoresist damage and residue on the edge were greatly reduced. Third, since the SiO etches, a sloped profile could be formed by tilting the substrate and controlling the etch rate with the CF_4/O_2 concentration.

Unsatisfactory tunneling characteristics (excessive leakage and a smeared gap) led to the attempt to ion-mill a tunneling edge in process NbN5. It is worth mentioning, though, that regardless of whether the edge was etched or milled it was exposed after etching to the ion-gun clean step to remove the native oxide. Nb and NbN will both oxidize in air and this layer must be removed. Thus, it is difficult to infer the effects on the tunneling performance of the RIE etch and the ion mill separately Etch rate data supplied with the ion gun from Ion Tech Inc. was used as a starting point to determine an appropriate SiO thickness. The SiO etched at approximately 5 Å/s, while the data sheet gave a rate of 4 Å/s. An Al_2O_3 milling mask produced with an e-beam evaporator was used next. It was found that a much slower etch rate of the mask resulted in approximately 0.1-0.25 Å/s rates when Al_2O_3 is used.

Figure 3-5 is a photograph of a completed NbN die. Two complete devices are on the die, which measures 6.75 x 6.5 mm. Figure 3-6 is a close-up of the actual junction. The top line is the bottom electrode while the overlapping stub is the top electrode. The numbers beside the junction indicate the width of the top electrode in microns.

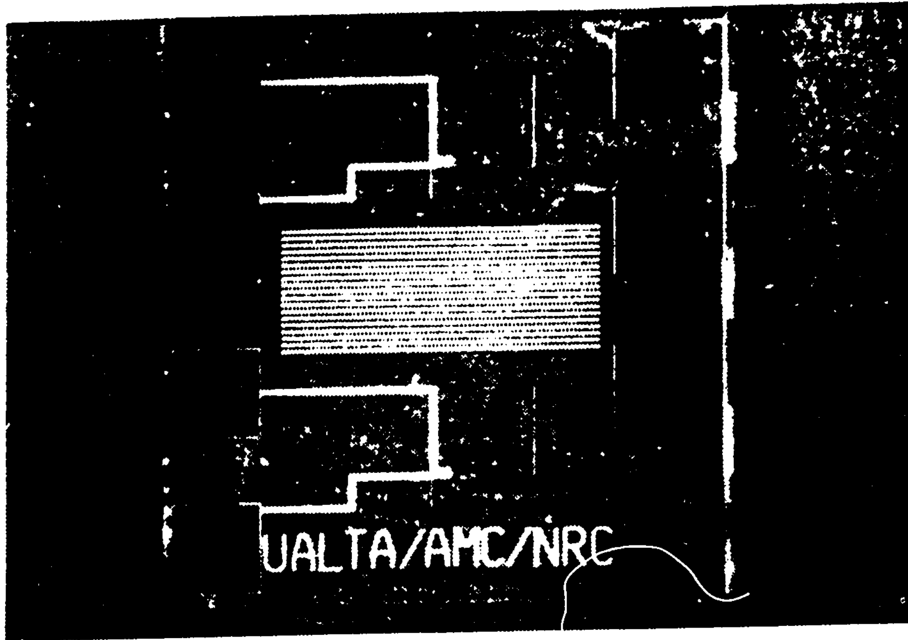

Figure 3-5 A completed die sawn from the substrate and ready for testing. Two completed devices are on one die.

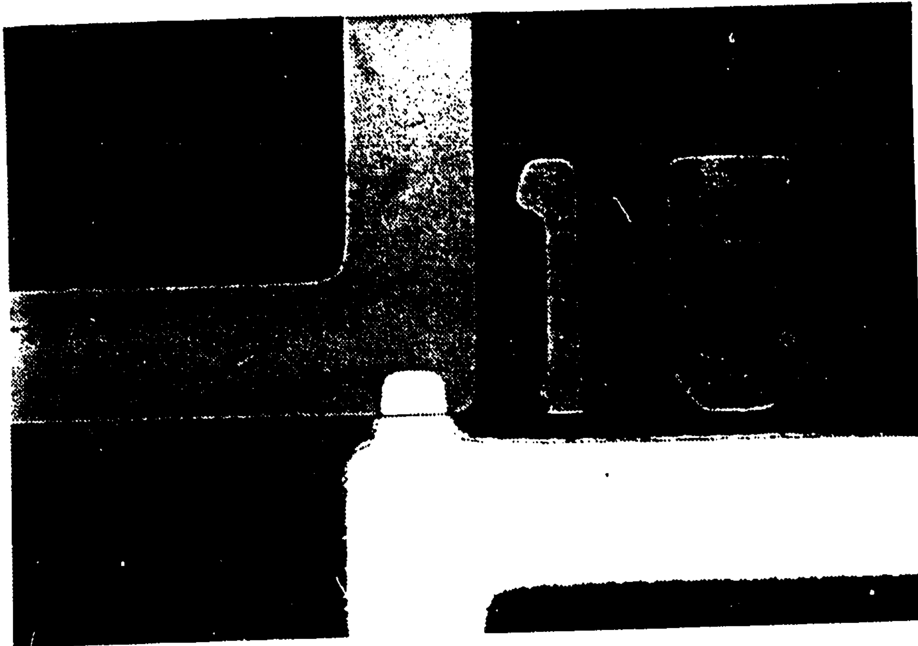

Figure 3-6 The junction area is visible in this photograph. This junction area is approximately 1.5 $(\mu m)^2$.

3.3 NbN SIS Device Results

A reactive ion etcher was used to produce the edges in all NbN fabrication runs. Since the junctions produced were short-circuited, a post-deposition cure was used to try to seal possible pinholes in the tunneling barrier. MgO sputtering time was increased to produce a thicker barrier. For resulting non-shorted junctions on each separate process run, the I-V characteristic was smeared out. Figure 3-7 is an I-V plot of a typical junction produced which was not short-circuited. It can be seen that while this junction was not shorted, the gap was severely smeared out so that only a slight non-linearity remains. The gap voltage for NbN should be near 5 mV, whereas the point of greatest non-linearity was observed near 2 mV. Since junctions produced with NbN could either be shorts or resistors for the same deposition conditions of MgO, the inconsistent behavior of the barrier could be attributed to roughness at the interface. As previously mentioned in chapter 1, any three-dimensional spatial variations of the electrode crystal (non-stoichiometric material, roughness, grain boundaries, etc.) will decrease the superconducting gap energy. If the disruptions of the lattice near the superconductor-insulator interface have a spatial extent longer than the coherence length, then a "smearing" of the gap may occur. Attempts to produce a smoother interface were not successful in improving junction quality. These attempts included reducing the plasma potential in the RIE by increasing the etch pressure, using shorter ion-gun cleaning times and decreasing the sputter etch angle to decrease the component of ion energy perpendicular to the tunneling edge. None of these techniques proved effective and the problems encountered led to experimentation with a longer coherence length material, Nb.

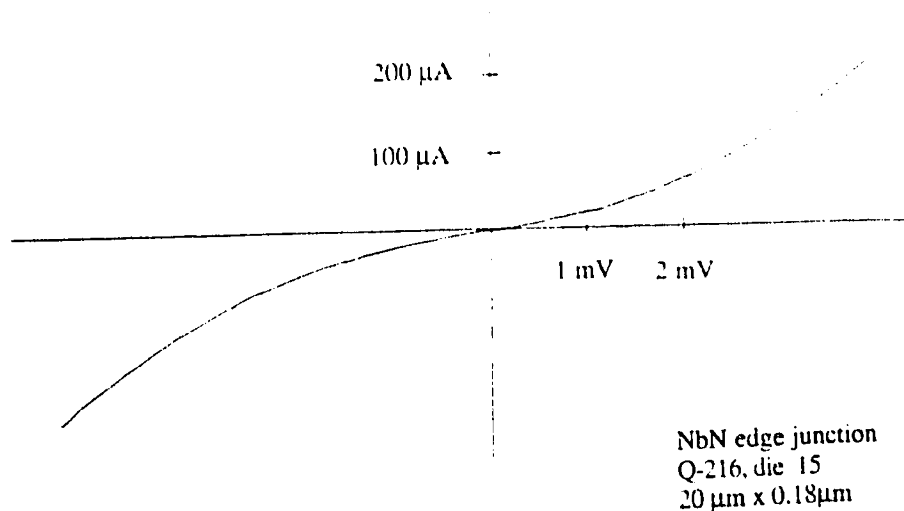

Figure 3-7 DC I-V curve of an NbN/MgO/NbN SIS edge junction.

The sputtering conditions for the junction of figure 3-7 were as follows:

Base electrode

Base pressure 5×10^{-7} Torr

Current 2 A

Voltage 364 (after 10 minute burn-in)

Argon flow 18.6 sccm

N_2 flow 4.9 sccm

Argon pressure 5.0 mTorr

Sputtering rate 14 Å/min

Thickness 5.69 kÅ (Alphastep)

Ion-gun clean

Exposure time 90 s

Pressure 8×10^{-5} Torr

Ion energy ~ 500 eV

MgO rf sputter deposition conditions

Power - 100 W

Argon flow - 23.8 sccm

Pressure - 5 mTorr

DC plasma potential - 240 V

Pin-hole cure - 21.1 sccm of O_2 at 10 mTorr

Counter-electrode

Current - 2A

N2 - 4.9 sccm

Thickness- ~3.25 kÅ

Voltage 359 (@ 10 minutes)

Chapter 4

Nb/MgO/Nb Edge Junction Fabrication and Testing

4.1 Nb fabrication

Following the unsuccessful attempts to fabricate NbN edge junctions, it was decided to attempt fabrication of Nb edge junctions. The longer coherence length of Nb (~30 nm vs. ~3 nm for NbN) greatly eases the restriction on the tunnel barrier smoothness. Fortunately, no major process variations were necessary in switching to Nb. Sputtering Nb is much simpler; the only variable affecting film quality directly is the argon pressure which was again optimized to produce low stress films. Typical pressures used were 8 mTorr with 40 sccm argon flow. The system pressure was modified for a fixed sputter gas flow using a variable orifice which controlled the pumping speed.

One difficulty in using Nb is the fact that the bottom electrode will oxidize in air, to a depth of around 20 Å, effectively increasing the tunneling barrier thickness to a net unknown thickness. Thus, prior to depositing the MgO tunneling barrier, this oxidized layer must be removed while in vacuum. The only method available to do this is an ion gun mounted in the bottom chamber. The major drawback of having to expose the junctions to air (between RIE edge definition and barrier deposition) is encountered at this step since removing the oxide necessarily roughens up the barrier. Furthermore, a limitation of the ion gun used (Ion Tech Inc. 3 cm source) is that it cannot be operated stably at ion energies much below 500 eV. Energies of this range may induce damage while removing oxidized Nb. In comparison Leduc et. al. used 150 eV for their edge-cleaning step [6]. The ion clean process will be discussed later in the context of the quality of junctions produces. The following pages, (figures 4-1 and 4-2) summarize the two main processes used to produce Nb/MgO/Nb edge junctions.

Figure 4.1 Nb Edge Junction Fabrication Process #1

1. Sputter Nb base layer.

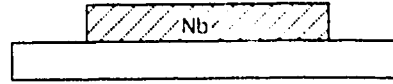

2. SiO isolation layer evaporated and patterned using reversal of mask1. (Photoresist lift-off used).

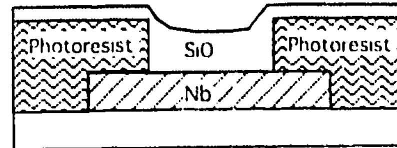

3. Remove pr. RIE SiO/Nb stack, tilting substrate to form sloped edge. SiO used as etching mask.

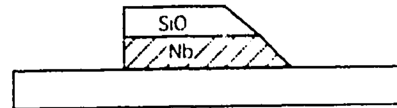

4. Rf sputter MgO tunneling barrier.

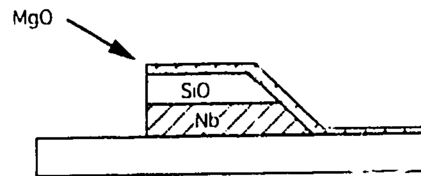

5. Deposit Nb counterelectrode.

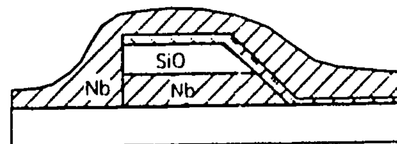

6. Pattern counterelectrode with mask 2 and RIE etch.

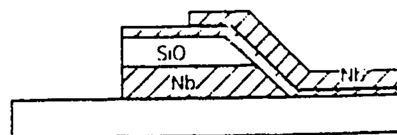

7. Deposit SiO passivation layer.

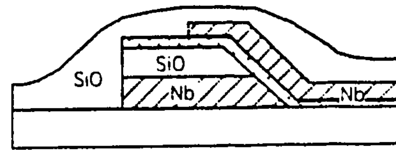

8. Pattern passivation layer with mask 3 and BOE etch through to bonding pads.

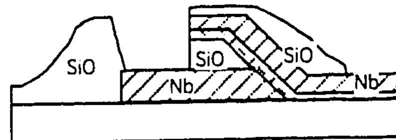

9. Dice wafer and test.

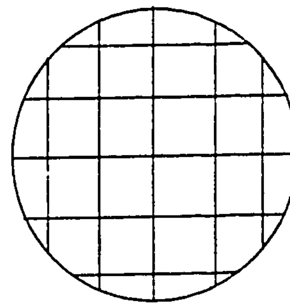

Figure 4.2 Nb Edge Junction Fabrication Process #2

1. Sputter Nb base layer.

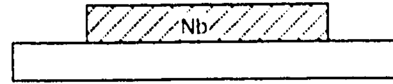

2. Al_2O_3 isolation layer e-beamed and patterned using reversal of mask 1. (Photoresistlift-off)

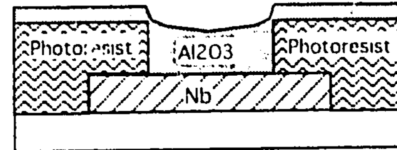

3. Remove pr. The tunneling edge is ion-milled with and argon ion-gun. The substrates are again tilted to form a sloped edge.

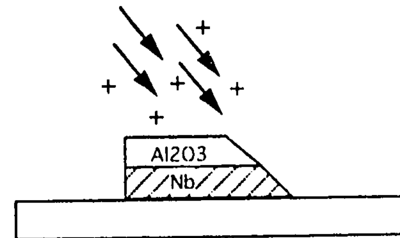

4. Rf sputter MgO tunneling barrier.

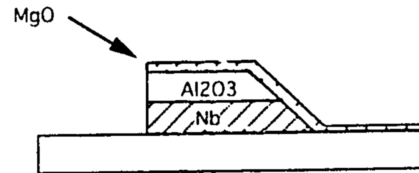

5. Deposit Nb counterelectrode.

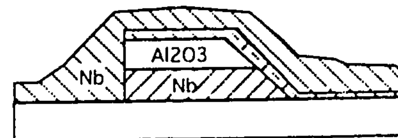

6. Pattern counterelectrode with mask 2 and RIE etch.

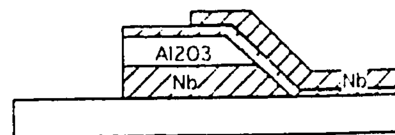

7. Deposit SiO passivation layer.

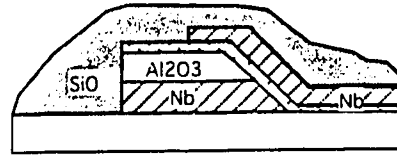

8. Pattern passivation layer with mask 3 and BOE etch through to bonding pads.

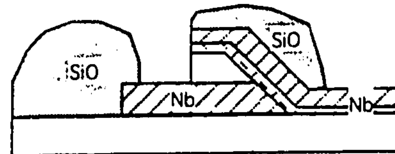

9. Dice wafer and test.

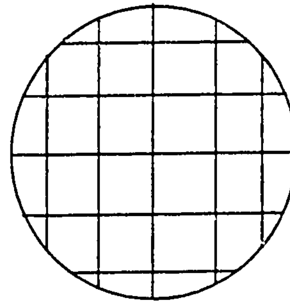

4.1.1 Photoresist lift-off

The first mask defining the bottom electrode was copied onto a 4"x 5" piece of glass and then the negative of this image was copied onto a second mask blank, producing the reversed image to do photoresist lift-off of the SiO during the first photolithographic step. This was done to avoid having to wet etch the SiO in buffered oxide etch (BOE). Wet etching tends to be an isotropic process for amorphous materials which would leave an undesirably rounded profile of the isolation layer. Much sharper profiles resulted from lift-off. After the lift-off film was evaporated, the photoresist was removed by immersing the substrates in a petri dish of acetone. Ultrasonic agitation can be used to speed up the process. It was found that sputtered MgO did not grow effectively in the photoresist lift-off well prior to attempting evaporation. Instead, good coverage of the SiO in the lift-off well was enhanced by the planetary rotation apparatus of the thermal evaporator.

For the process in figure 4-2, an Al_2O_3 milling/isolation mask was evaporated with an electron gun because the SiO etched too fast in the ion-gun. The evaporation rate of Al_2O_3 was kept low (near 3 Å/s at 75 mA current) after discovering that the photoresist was excessively heating up as the film was being deposited and becoming difficult to remove. It was necessary to scrub the substrates with a q-tip to completely remove heated photoresist.

4.1.2 RIE Etch Process

Soon after switching to Nb, an RIE became available for experimental use. A possible cause of the random behavior of the NbN junctions could be that the tunneling edge was nearly vertical and therefore difficult to coat uniformly by sputtering. Saserath et. al. used varying concentrations of CF_4 and O_2 to produce a sloped edge [18]. However, this group used photoresist as an etch mask, which can lead to other problems such as junction contamination and changes in oxygen concentration (since photoresist is etched by O_2). To avoid this problem, the junction isolation mask was also used as the etching mask. A sloped edge was formed by tilting the substrates with respect to the bottom electrode. Etch variables were chosen to enhance anisotropy. Low power levels of 60 W and pressures near 60 mTorr were found to work reproducibly. Repeated experimentation led to gas concentrations of 5% O_2 and 90% CF_4 in order to produce reasonable profiles, shown in figure 4-3. In this photomicrograph the SiO/Nb stack is clearly visible. At the above gas concentrations, the etch rate is about 60 nm/min at 60 mTorr and 60 W. The edge of substrates always cleared quicker than the central portion with this RIE, so a slight overetch at the edges of the wafer was unavoidable.

4.1.3 Ion beam milling Nb

There are essentially two main techniques to form the tunneling edge; by RIE etching [31,32] discussed above, and by ion milling [19,20]. Both methods have their adherents. Lichtenberger et. al. performed a study to discern the effect of the ion-voltage on the quality of their Nb and NbN edge junctions. This group found a strong correlation between NbN junction quality and the acceleration voltage used (voltages below 125 V gave best results) to remove the damage caused by the cutting step, but they could find no such relationship for Nb junctions. They attributed this result to the difference in coherence lengths for Nb and NbN and also to the possibility of the ion bombardment altering the NbN stoichiometry. In order to try to reduce the leakage

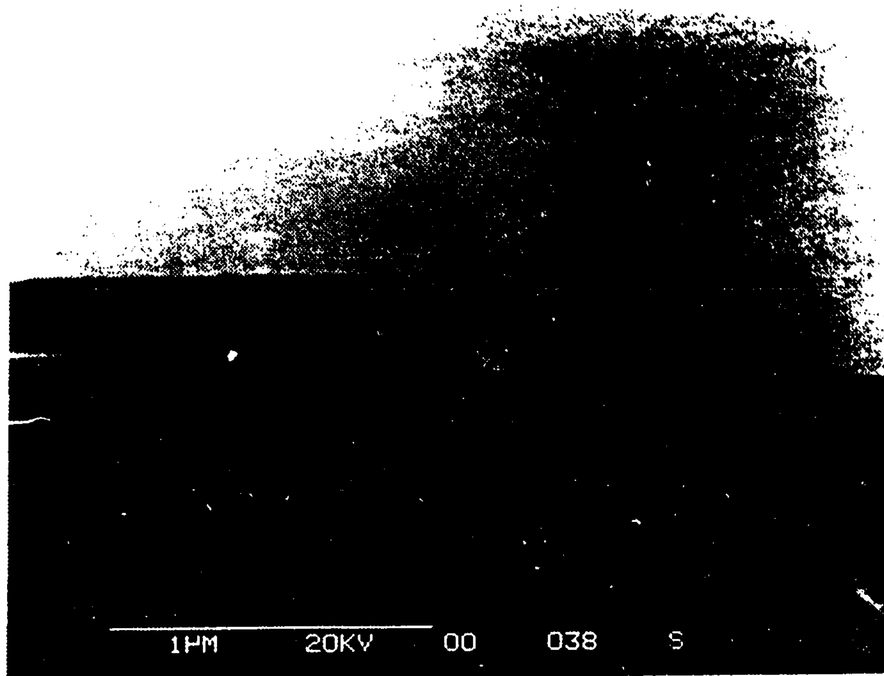

Figure 4.3 RIE of Nb/SiO stack. Etch conditions were 5%/ O2, 90% CF4, 60 mTorr pressure and 60W rf. Etch time was approximately three minutes.

currents observed with our RIE produced edge junctions, an Nb edge was ion milled using a commercial 3 cm ion gun. This ion gun could not be operated stably below about 500 eV ion acceleration energy, therefore it was not possible to experiment with the effects of varying the ion-sputter voltages on the junction quality. Another difficulty with the edge cutting step was the fact that it was not possible to have the edge cleaning step at the same angle as the cutting step (about 18°) because this would not allow the edge to be perpendicular to the MgO sputter flux in the next step. (The best quality, densest MgO films grow on surfaces perpendicular to the incoming sputter flux). Two different materials were used as milling masks during the processing. Thermally evaporated silicon monoxide was first used. The ion-milling rate of SiO was found to be between 4 and 5 Å/s while the rate for Nb was around 0.5 Å/s. One minute of ion beam exposure to the film was used. Evaporated SiO was not found to be satisfactory because its thickness must be much larger than the bottom electrode, because of its high etch rate. Since the milling mask must have a slow etch rate as well as electrically isolate the junction, the choice of materials is rather limited. However, e-beam evaporated Al_2O_3 was found to work satisfactorly, with an etch rate between 0.1-0.2 Å/s. The Al_2O_3 was deposited at a base pressure of 1.5×10^{-7} mTorr. The evaporation rate was kept low (near 3.0 Å/s at 75 mA electron current) to prevent the lift-off photoresist from heating up excessively and making it difficult to remove.

4.2 Summary of Nb SIS Junction Fabrication Experiments

Seven Nb fabrication runs were performed and are summarized in Table 4.0. Initial success in producing SIS junctions occurred with the first batch, although there was significant leakage. Batch Nb5 was essentially a replication of Nb4 to confirm control over the process. One of the first process parameters optimized in batch Nb4 was the MgO sputter time. The MgO was sputtered from a 2" target (99.95%) using an K.J. Lesker Torus 2C sputter gun. The gun magnets were weak and the rf plasma

was ignited by a dc plasma from another gun. At an argon sputter pressure of 7 mTorr (40 sccm flow) and 100 W rf, the optimum sputter time was found to be 100 s. Despite high leakage, junctions were produced with encouragingly high critical current densities, up to 20 kA / cm^2. In order to try to reduce the leakage, a dc oxygen plasma was struck in the chamber after deposition of the MgO to oxidize any pinholes in experiment Nb6. (Later in run Nb8b, various lengths of oxidation time were used.) In run Nb7, the MgO was sputtered with oxygen added to the discharge to try to oxidize any magnesium excess during sputtering. The result of O_2 plasma oxidation and reactively sputtering in an O_2 environment was that the junction gap voltage became progressively more smeared and leakage increased.

TABLE 4.0

Nb/MgO/Nb SIS JUNCTION FABRICATION EXPERIMENTS

Batch Nb4

Sputter Nb/MgO/Nb. Deposit MgO for varying times to deduce optimum thickness. Some junctions produced, but leakage current was higher than desired.

Batch Nb5

Replicate above initial success. Working junctions produced similar to Nb4.

Batch Nb6

Plasma oxidation of all facets using Al electrode after MgO sputter. Some junctions produced. Others were superconducting shorts.

Batch Nb7

MgO reactively sputtered in O_2, (keeping sputter pressure constant) to try to reduce the high leakage currents. No tunneling seen, mostly superconducting shorts.

Batch Nb8a

Plasma oxidation of varying lengths of time tried. Observed increased zero voltage current or produced resistors.

Batch Nb8b

Al_2O_3 milling mask used. Beam only etches part of the two substrates put on both facets. Few dies to test. No junctions.

Batch Nb9

Lifted off Nb. One substrate per facet for better centering in the ion-gun flux. No tunneling seen. Reasons unknown.

4.3 DC Nb/MgO/Nb Test Results

Table 4.1 documents the results of the process runs that yielded working junctions. Not all junctions were tested and yields varied sporadically between runs, so these parameter values can be assumed to be those of the better functioning junctions. R_n is the normal state resistance, which is the slope of the I-V characteristic above the knee. The sub-gap resistance, R_{sub}, is a measure of the gap leakage, measured here as the quotient of the gap voltage and the corresponding current, where the current rises sharply. The gap voltage, Δ_Σ , is the voltage at the knee of the I-V curve. The critical current is taken as 0.7 times the quasiparticle current rise at the energy gap voltage: $I_c = 0.7\ \Delta I_{ss}$. Figures 4-4 a and b are pen-plots of some of the better dc I-V curves obtained during run Nb4. Large sub-gap leakage is clearly evident. The gap voltage of the best devices produced in Nb4, about 2.7 mV, compare well to the theoretical value of about 3.0 mV. The voltage was ramped in both directions to show any hysteresis effects.

Table 4.1 DC I-V tests of Nb/MgO/Nb Junctions

Batch	Area $(\mu m)^2$	$R_n(\Omega)$	$R_{sub}(\Omega)$	$\Delta_\Sigma(mV)$	$I_c(\mu A)$
4	0.9	15	38	2.8	140
4	27	36	23	2.7	49
5	2.7	5	39	2.4	336
5	0.9	12	54	2.4	140
6		40	177	2.4	42
6		37	37	2.4	46
6	2	12	51	2.3	140
6	2	10	38	2.5	168
6	0.5	18	66	2.5	95
8a	1	12	55	2.7	140
8a	2	24	80	2.4	70

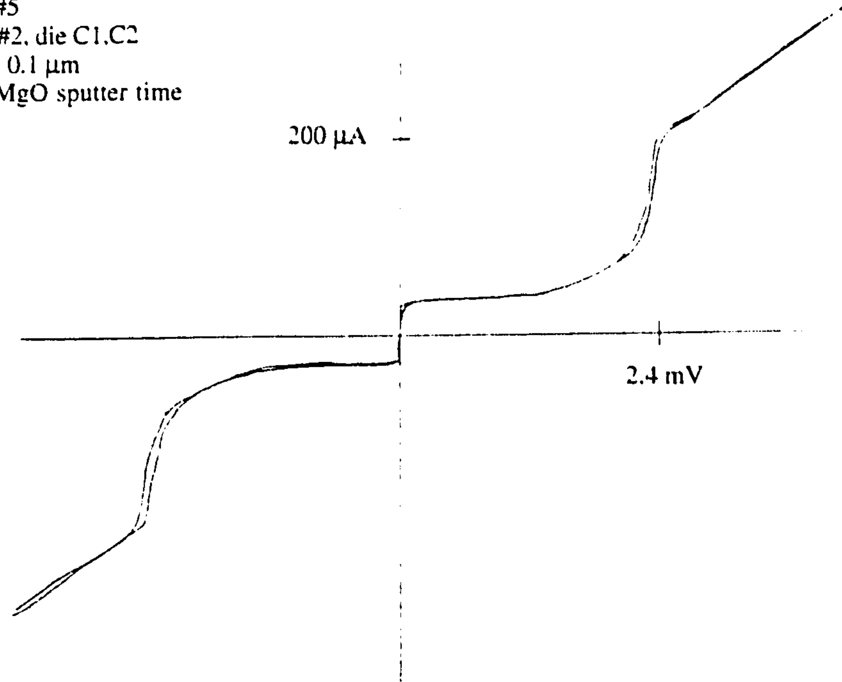

Figures 4-4a and b DC I-V plots of Batch #5 Nb/MgO/Nb edge junction.

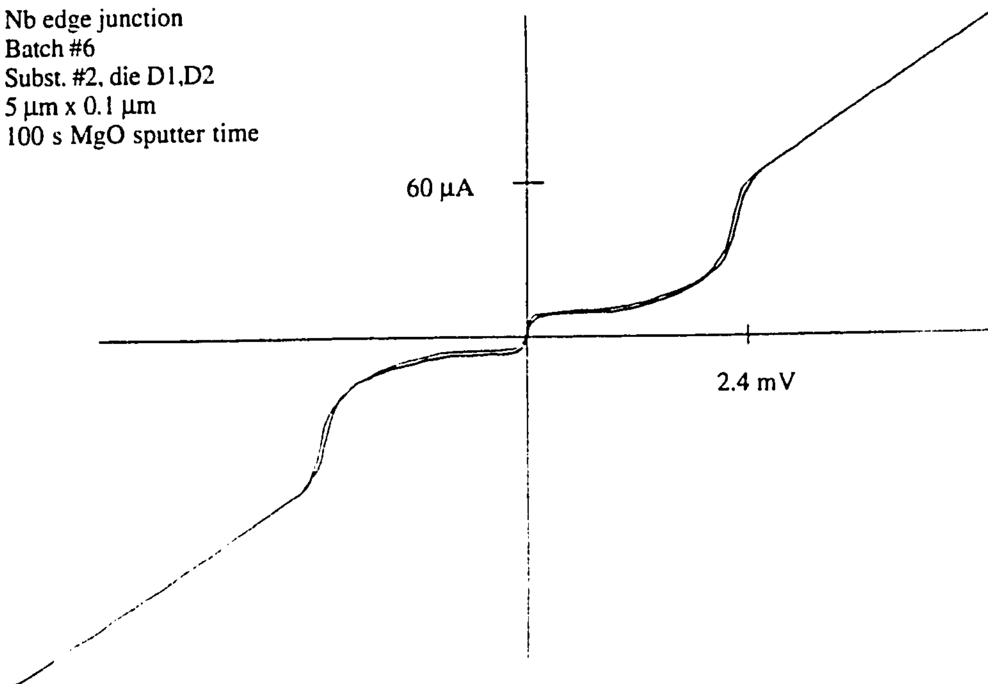

An attempt was made to measure the tunneling barrier thickness using a mechanical profilometer (Tencor Alphastep 100). MgO was sputtered on lines of accurately known thickness and bare glass substrates. The sputtered thickness of the MgO was taken as the difference of the (line + MgO) - line. The roughness of the glass substrate was reduced by averaging over many sets of lines. The relative rather than the absolute thickness of the thin MgO layer is more accurate since the resolution of the profilometer is near the sputtered thickness (~200 Å). The results are displayed in figure 4-5. This is a very crude method of performing such a measurement; however it is useful for a rough idea. From this plot, 100 s of sputtering time yielded insulators approximately 120 Å thick.

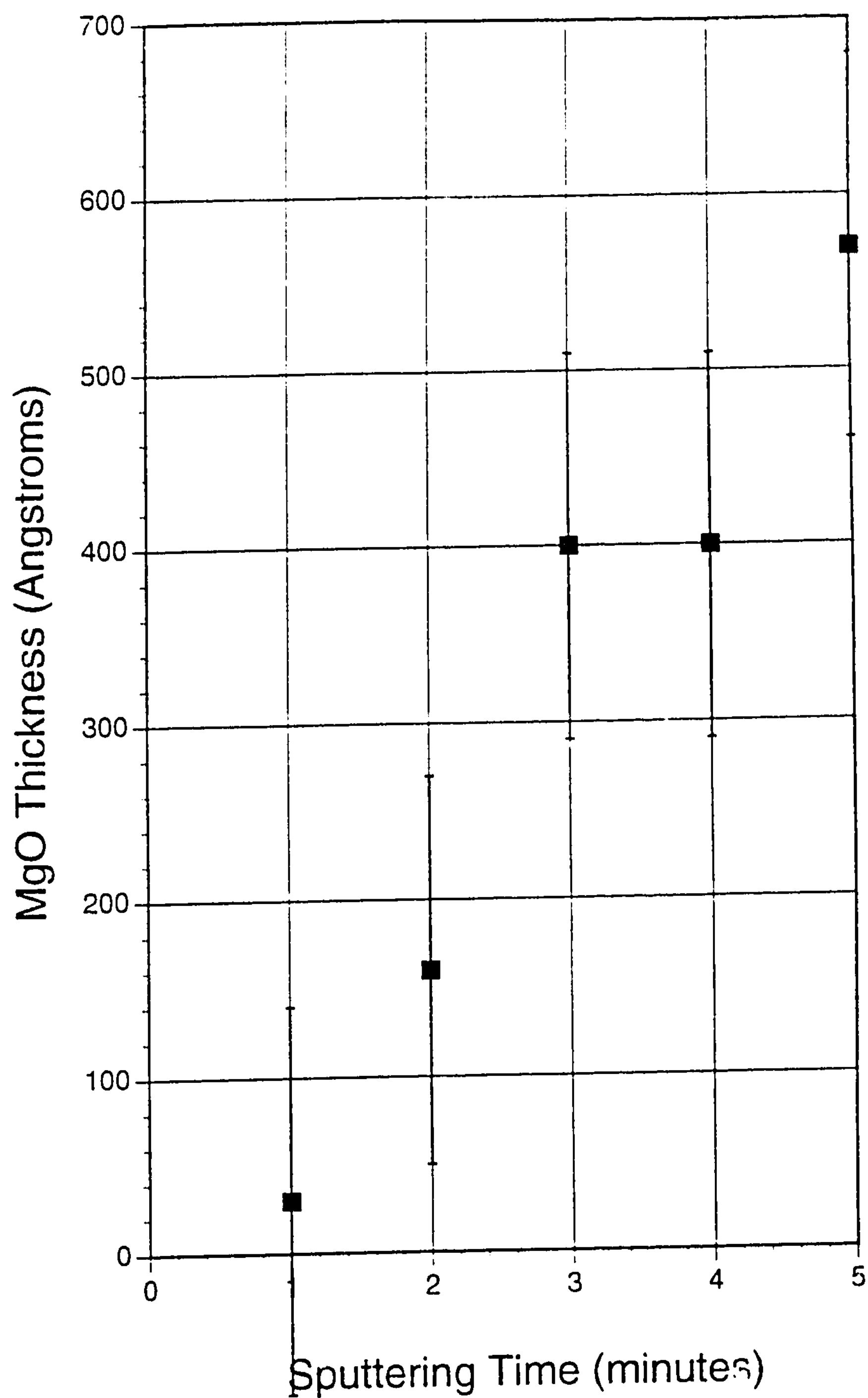

Figure 4-5 Thickness measurements of sputtered MgO films at the deposition conditions used to produce insulator barriers.

4.4 Discussion of Test Results

After it was demonstrated that tunneling behavior was occurring in Nb junctions, the main research focus was trying to reduce the leakage. Gross leakage could occur through a discontinuous barrier, or through non-insulating material. When NbN is used as a superconducting material, a common technique for sealing "pinholes" in the MgO barrier is to expose the barrier to an O_2 ambient to fully oxidize a magnesium excess or the underlying exposed NbN [7, 33].

Attempts to reduce the subgap leakage were made by three techniques. An O_2 plasma was struck in the chamber after the MgO deposition, O_2 was flowed into the chamber without a plasma, and O_2 was added to the MgO sputter discharge. The results from all three techniques yielded similar results. Figures 4-6 a and 4-6 b document these results, showing the gap completely smeared out after eight and a half minutes of plasma oxidation. If the oxidation was simply increasing the thickness of the insulating barrier, the subgap current should drop dramatically, since the tunneling current is exponentially dependent on the barrier thickness. What resulted was an increase in leakage current and a smearing of the gap voltage. There are several known stable oxides of niobium including an insulator, a low T_c superconductor and a semiconductor. All of these phases could be simultaneously present. Oxidizing Nb could result in forming a partly oxidized and irregular Nb region of unknown composition and properties. If the oxide of Nb was conducting, superconductor-insulator-normal (SIN) tunneling could result. What would be expected in this case is a less sharp turn-on of the tunneling current at the gap voltage since there are no singularities in the density of states at the band edge for a normal metal. The I-V characteristics in figure 4-6 seem to illustrate this. Figure 4-7 shows the measured critical current vs. sputter time for non-oxidized MgO barriers. Despite the scatter, the trend is a logarithmic reduction in tunneling current with a linear increase in barrier thickness (ie. sputter time), as expected from electron tunneling phenomena. Thus the tunneling behaviour of the barriers is appropriate but the oxidation process

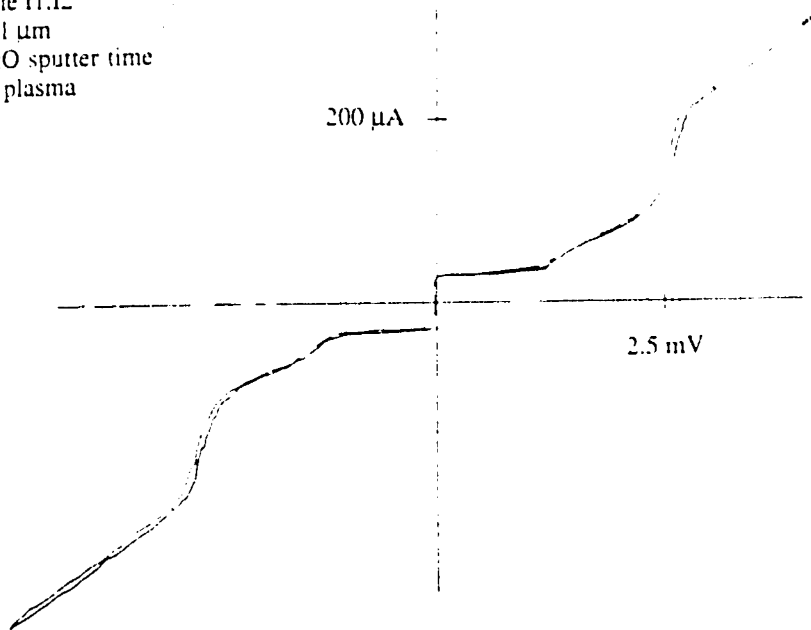

Figures 4-6a and b DC I-V plots of Batch #8a Nb/MgO/Nb edge junction with post-deposition plasma oxidation.

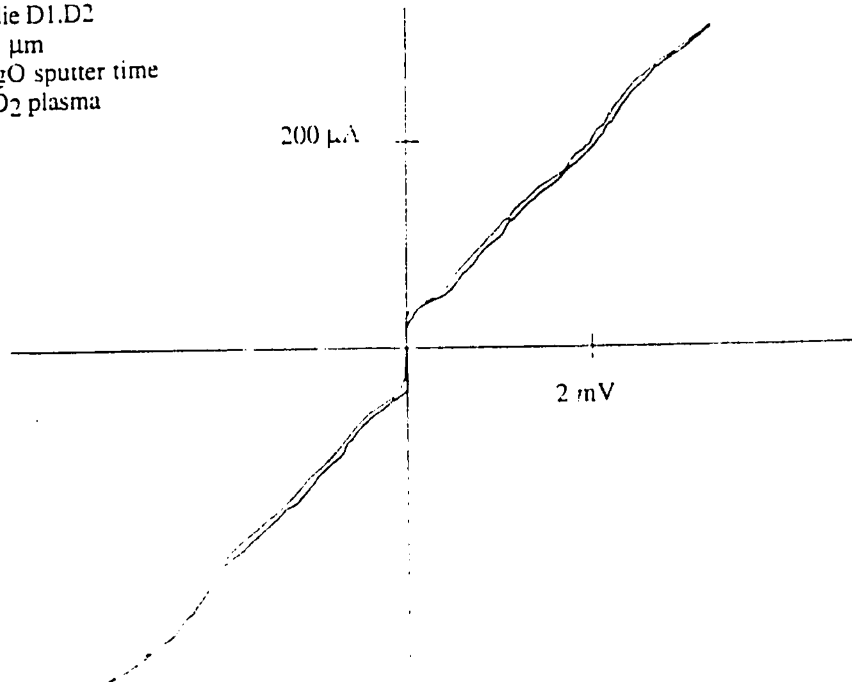

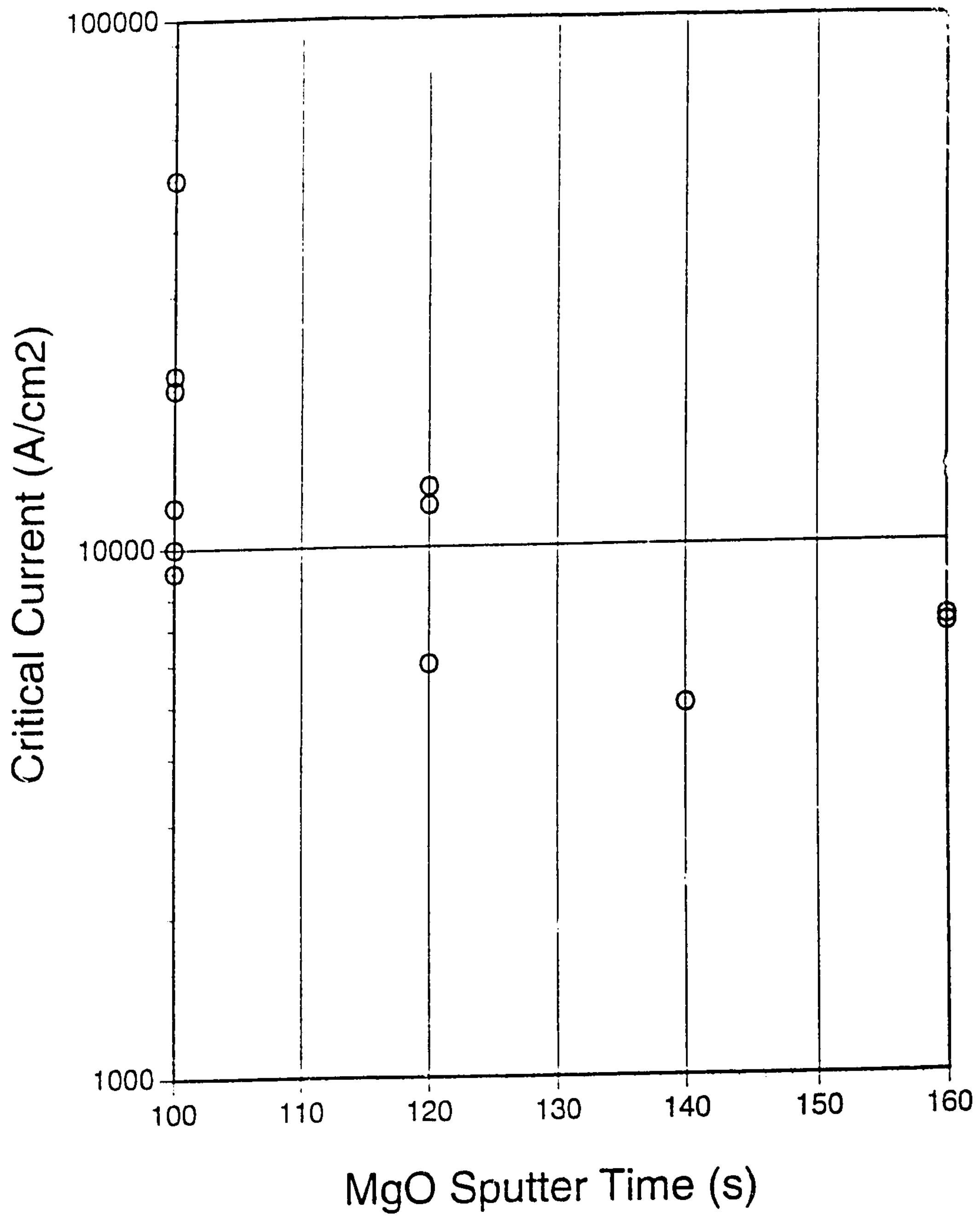

Figure 4-7 Critical current vs. sputter time for junctions without a post-MgO oxidation process.

may alter the conductivity of the material at the barrier/superconductor interface.

The current densities of the junctions produced compare favorably with those produced by other workers. Broom reported current densities of at least 20 kA/cm^2 while Kleinsasser had values between 10^4 - 10^5 A/cm^2 [9,34]. The best junctions made in this study were 5 x 10^5 A/cm^2. In light of these respectable current densities, it would be interesting to know the performance of these Nb/MgO/Nb edge junctions, if the insulator quality was optimized.

An atomic force microscope (AFM) was used to try to measure the surface roughness of edges produced by ion-milling and RIE. While the vertical travel of the AFM was sufficient to traverse the edge, it was impossible to scan the edge because the operator could not discern where the edge began exactly. The scan was completed across the top of the isolation layer, to try to get an estimate of the surface irregularities. This scan indicated that the RIE etched sample had roughness up to 140 Å and the ion gun etched sample left pits up to 70 Å in depth. This surface roughness, if similar on the edge, would render it impossible to deposit a smooth and continuous 50-100 Å thick insulator layer.

Chapter 5

Conclusion

5.1 Summary

Sub-micron area Nb/MgO/Nb Superconductor-Insulator-Superconductor (SIS) tunneling edge junctions were fabricated with high critical current densities. Similar geometry NbN/MgO/NbN edge junctions exhibited very little tunneling phenomena. These junctions are not suitable for high-frequency mixer applications because of a reduction in their nonlinear I-V characteristics. The nonlinearity of these junctions was reduced by two effects.

First, sub-gap leakage currents for both the NbN and the Nb edge junctions were unacceptably high. It is hypothesized that the cause of the leakage was conduction across a rough insulator interface through "pinholes" in the MgO barrier. An linear increase in MgO thickness decreased the critical current exponentially with little or no change in leakage, implying that the surface roughness was too large to cover with a barrier of the preferred thickness. An initial Atomic Force Microscopy (AFM) analysis of the Al_2O_3 milling mask indicated that the surface irregularities vary from 70 - 140 Å, similar in thickness to the insulating barrier.

Secondly, the turn-on of the tunneling current at the gap voltage was rounded to a large extent. Three different methods were attempted to try to reduce the leakage current by providing a continuous insulating barrier, with the result that the gap was more severely rounded and the leakage current was increased. A probable cause for the rounding was that the oxidation formed the conducting oxide of niobium. This would result in superconductor-insulator-normal (SIN) tunneling, which would result in a rounded gap because there are no singularities in the density of states at the band edges for a metal. The inability to preferentially form the insulating oxide of niobium

limits the value of a post-deposition barrier oxidation. The cause of the increased leakage with oxidation could be a change in composition at the barrier.

The use of MgO as a tunneling barrier with Nb edge junctions, is, to the best of my knowledge, unique. The advantages of the edge-geometry may yet be combined with the high current densities demonstrable here to produce a good superconducting mixing element.

5.2 Suggestions for Future work

The first concern to be addressed in any follow-up work producing edge junctions with either Nb and especially NbN is surface roughness. AFM studies need to be done to ascertain the size of the surface irregularities and the ability of a low-energy ion clean to remove the damage. An ion-gun capable of lower operating voltages should be tried. Lower ion-milling energies could be used to try to produce a smoother interface with less damage. One investigation worth performing is to see what the effects of varying angles of the substrate to the ion beam have on junction quality during the edge cutting step.

A second issue not directly investigated but worth considering is using oxidized aluminum for the tunneling barrier. A wealth of data exists in the literature about producing $Nb/Al/Al_2O_3/Nb$ planar junctions and this could be exploited in producing edge junctions. The growth modes of MgO on Nb and NbN are still uncertain and the success of oxidized aluminum barriers should be used. This would necessitate a re-design of mask 1 used to produce tunneling edges.

A final experiment would help to clear up the mystery of why a plasma oxidation did not reduce the leakage in the junctions. This would be to simply oxidize the cleaned edge in the sputter system to try to observe tunneling with a native oxide barrier. If the junction was merely resistive, the native oxide would be deemed insufficient for an insulating barrier. If t tunneling is observed, the question why pinholes in NbN and Nb cannot be oxidized would have to be answered.

REFERENCES

1 W.M. Kelly and G.T. Wrixon *Infrared and Millimeter Waves*, (Academic, New York,1979) Ch. 3 p.77.

2 T. J. Phillips and D.P. Woody, "Millimeter and submillimeter wave receivers", Annual review of astronomy and astrophysics, vol. 20, p. 298, 1982.

3 J.R. Tucker, IEEE QE-15, p. 1234, 1979.

4 L. N. Cooper, Phys. Rev., vol. 104, p.1189 (1956).

5 J.H. Hinken, *Superconductor Electronics*, (Springer-Verlag, New York, 1989) Ch. 2 page 32.

6 J.A. Stern Ph.D. thesis, "Fabrication and testing of NbN/MgO/NbN tunnel junctions for use as high frequency heterodyne detectors" page 10.

7 B.D. Hunt, H.G. Leduc, S.R. Cypher and J.A. Stern, "NbN/MgO/NbN edge-geometry tunnel junctions", Appl. Phys. Lett. 55 (1) p.81-83, 1989.

8 R.H. Havemann, "Photolithographic fabrication of thin-film metal-oxide-metal diodes with submicrometer-square junction areas", J. Vac. Sci. Technol 15 (2) p. 389-391, 1978.

9 R.F. Broom, A. Oosenbrug, W. Walter, "Josephson junctions of small area formed on the edges of niobium films", Appl. Phys. Lett. 37 (2) p. 237-239, 1980.

10 S.I. Raider, R.E. Drake, "Nb/Nb oxide/Pb-alloy Josephson Tunnel Junctions", IEEE Trans. Vol. MAG-17, No. 1 p. 299-302, 1981.

11 A.C. Callegari, R.A. Buhrman, "Millimeter wave mixing with submicron area tunnel junctions", J. Appl. Phys. 53 (2) p. 823-827, 1982.

12 L. Jackel, E. Hu, R. Howard, L. Fetter and D. Tennant, "Submicron Tunnel Junctions", IEEE Trans MAG-17 p. 295-98, 1981.

13 J. Talvacchio and A.I. Braginski, "Tunnel junctions fabricated from coherent NbN/MgO/NbN and NbN/Al_2O_3/NbN structures", IEEE Trans MAG-23 p. 659-61, 1987.

14 H.G. Leduc, A. Judas, S.R. Cypher and B. Bumble,"Submicron area NbN/MgO/NbN tunnel junctions for SIS mixer applications", IEEE Trans MAG-27 p. 3192-95, 1991.

15 A.W. Lichtenburger, C.P. McClay, R.J. Mattauch and M.J. Feldman, "Fabrication of Nb/Al-Al_2O_3/Nb junctions with extremely low leakage currents", IEEE Trans. on MAG-25 p. 1247-50, 1989.

16 RMC Inc., Tech. Div., 4400 S. Santa Rita Ave., Tucson, AZ 85714

17 X.F. Meng, R.S. Amos, A.W. Lichtenburger, R.J. Mattauch and M.J. Feldman, "NbN edge junction fabrication:edge profile control by reactive ion etching", IEEE Trans MAG-25 p.1239-42, 1989.

18 J.N. Sasserath and J. Vivalda, "Sloped niobium etching using CF4 and O2", J. Vac. Sci. and Technol. A8(6) p.3914-19, 1990.

19 A.W. Lichtenburger, M.J. Feldman, R.J. Mattauch and E.J. Cukauskas, "The effects of ion gun beam voltage on the electrical characteristics on NbCN/PbBi edge junctions", IEEE Trans MAG-25 p.1243-46,1989.

20 S.S. Pei and R.B. van Dover, "Ion beam oxidation for Josephson circuit applications", Appl. Phys. Lett. 44(7) p.703-5, 1984.

21 J.H. Hinken, p. 60.

22 W. Anacker, "Computing at 4 degrees Kelvin", IEEE Spectrum, May 1979, p. 26.

23 B. Chapman, Glow Discharge Physics: Sputtering and Plasma Etching, p179, (John Wiley and Sons, New York, 1980).

24 W. D. Westwood, "Reactive Sputter Deposition", in *Handbook of Plasma Processing Technology*, edited by S.M. Rossnagel, J.J. Cuomo and W.D. Westwood (Noyes, New Jersey, 1990) p. 233.

25 D.M. Manos and D.L. Flamm eds., *Plasma Etching an Introduction*, (Academic Press, Inc, New York, 1989.) Chapter 1 p 32.

26 G.S. Oehrlein "Reactive Ion Etching", in Handbook of Plasma Processing Technology, S.M. Rossnagel, J.J. Cuomo and W.D. Westwood, eds., (Noyes Publications, New Jersey, 1990).

27 K.L. Westra, M.J. Brett and J.F. Vaneldik "Properties of reactively sputtered NbN films", J. Vac. Sci. Technol. A 8 (3) p. 1288-1293, 1990.

28 Milton Ohring, *The Materials Science of Thin Films*, (Academic Press, San Diego, 1992), p. 429.

29 J. F. Vaneldik, K.L. Westra, D. Routledge and M.J. Brett "Target Hysteresis and film properties of sputtered NbN", J. Phys. D. 22 p. 1788-1790,1989.

30 T. Smy, R.N. Tait, and M.J. Brett, "Ballistic Deposition Simulation of Via Metallization Using a Quasi-Three-Dimensional Model", IEEE Trans. on Comp. Aided Design, Vol. 10, p. 132, 1991.

31 C.K. Hu, N. Mazzeo, S.J. Wind, D.J. Pearson and M.B. Ketchen, "Reactive ion etching of $Nb/AlO_x/Nb$ for Josephson technology", Thin Solid Films, 206, p. 151-155, 1991.

32 P.R. Brosious, "The role of Ar^+, CH_4^+, $O_4 2^+$ and backscattered Pb^+ ions during Nb/oxide/PbAuIn Edge Junction Fabrication", IEEE Trans. Mag 21 No.2 p. 118-121, 1985.

33 H.G. LeDuc, J.A. Stern, S. Thakoor, S.K. Khanna, "All Refractory NbN/MgO/NbN Tunnel Junctions", IEEE Trans. Mag-23, p. 864, 1987.

34 A. W. Kleinsasser, "Relationship between beam and junction parameters in ion beam processed Josephson devices", J. Appl. Phys. 57, p. 2577, 1985.

APPENDIX A

Optical Constants of Reactively Sputtered NbN Films

This appendix contains a manuscript accepted for publication in *Thin Solid Films*. Optical properties of NbN were studied at the beginning of this thesis research, in the hope that a better understanding of NbN would lead to fabrication of improved devices. This work is included as an appendix since it was part of NbN device development but had no direct bearing on the fabrication experiments.

Optical Constants of Reactively Sputtered NbN Films

M. W. Konevecki, K. L. Westra+, B. T. Sullivan*, K.E. Kornelson and M. J. Brett

Department of Electrical Engineering, University of Alberta, Edmonton, Alberta, Canada T6G 2G7

+ Department of Electrical and Computer Engineering, University of Manitoba, Winnipeg, Manitoba, Canada R3T 2N2

*Institute for Microstructural Sciences , National Research Council of Canada, Ottawa, Canada K1A 0R6

Abstract

NbN films of nominal thickness 1 μm and superconducting critical temperature of 14 K were prepared by reactive dc magnetron sputtering. A spectroellipsometer was used to measure the pseudo-dielectric constant $\langle\hat{\varepsilon}\rangle$ over the spectral interval 1.5 to 5.0 eV for films prepared at different nitrogen flow rates. Spectrophotometer measurements of film reflectivity were made, which confirmed the ellipsometer results.

1. Introduction

Niobium nitride thin films are of current interest as electrode materials for cryogenically cooled Josephson junctions because of their robust nature and relatively high superconducting critical temperature, T_c (near 17 K). The stable refractory characteristics of NbN makes it a more suitable material for use in superconductor-insulator-superconductor (SIS) applications, which require thermal cycling, than conventional lead junctions. To better understand NbN as a superconducting material for our SIS junctions, the optical constants of NbN were investigated. A spectroscopic ellipsometer was used to derive the optical constants over the energy range 1.5-5 eV (250-830 nm). These measurements were confirmed by spectrophotometry studies in the range 0.4 to 6.2 eV.

To the best of our knowledge this work reports the first measurement of NbN optical constants in the ultraviolet (UV) range 3.1 to 5 eV. However, there are two earlier reports of optical constants of NbN in the infrared and visible spectral regions [1-3]. Motolevich et. al. performed a study over the energy range .15 to 3.1 eV [1,2], whereas Tanabe et. al. used in-situ ellipsometry to correlate their film T_c with the ellipsometer parameters ψ and Δ at 2.0 eV [3]. The latter group also performed optical reflectivity measurements over the wavelength range 0.2-2.5 µm and used the Drude free electron theory to model the reflectivity. Our approach to characterizing NbN was to determine the dielectric constants from spectroscopic ellipsometry and from these measurements calculate the reflectivity, which was compared to the reflectivity obtained from a spectrophotometer.

2. Film Preparation and Characterization

The NbN films were deposited in a cryopumped dc planar magnetron sputtering system, described in detail elsewhere [4]. The films were deposited using a 12.7 x 20 cm niobium target (99.95% pure), with argon (99.9999% pure) and nitrogen (99.999% pure) as the sputter gases. The system was baked prior to deposition in order to reduce the base pressure to 5×10^{-5} Pa. The substrates used were Corning 7059 glass and 2.5 x 2.5 x 0.16 cm thick Heraeus Amersil Inc. Optosil 3 quartz plates. The substrates were cleaned in ultrasonically agitated acetone and isopropyl alcohol, and then blown dry with N_2. No intentional substrate heating was used during deposition.

It was reported previously that the films with the highest T_c were consistently deposited on the upper shoulder of the target voltage versus nitrogen flow hysteresis curve [4,5]. It was found that the argon pressure of 7.0 mTorr was a compromise between minimum stress and maximum T_c, as films at P_{Ar} = 5 mTorr were overly stressed and delaminated from their substrates. Four films were deposited on the upper shoulder of the hysteresis curve with decreasing nitrogen flow in order to bracket the previously discovered flow rates for the highest T_c. Table 1 summarizes the deposition conditions of the four films and some of their properties. The thicknesses of the films and the room temperature resistivities were measured using a Tencor Alphastep model 100 profilometer and a Veeco model 1200 four-point probe, respectively. The surface roughness and columnar microstructure of freshly cleaved samples were studied using a Cambridge Instruments S-250 scanning electron microscope (SEM).

3. Optical Characterization

A spectroellipsometer, described in detail elsewhere [6], was used to measure the complex reflectance ratio, ρ, of the films. An ambient substrate model

was used to determine the pseudo-dielectric function $<\hat{\varepsilon}> = <\varepsilon_1> + <\varepsilon_2>$ over the spectral range 1.5 to 5.0 eV. In this model, the films are assumed to be isotropic and homogeneous, and any surface roughness is neglected. The samples were measured approximately 72 hours after removal from the sputter chamber, and the results are shown in Fig. 1. The reflection spectra for the four films were measured over the wavelength range 200-3000 nm using a Cary 2415 spectrophotometer fitted with a dual beam V-W reflectance accessory. The reflectivity measurements were performed within 4 hours of removing the samples from the sputtering system. The angle of incidence of the light on the sample was 7° for this accessory. The accuracy of the spectrophotometer was evaluated by measuring the reflectivity of a freshly evaporated silver film 200 nm thick. The measured reflectance values were compared to tabulated values [7], and over the wavelength of interest the two spectra differed by less than five percent (relative to each other), with a slightly greater deviation in the region near 340 nm where the reflectance drops rapidly. The accuracy of the monochrometer was verified with a Didymium reference sample obtained from the National Institute of Standards and Technology in Gaithersburg, Maryland, with discrepancies found to be less than 1%.

4. Results and Discussion

Figure 2 is a cross-sectional SEM photograph of sample F4, which exhibits a columnar microstructure typical of all samples. Specifically, the films have a zone T structure as described by the structure zone model developed by Thornton [8,9]. Figure 2 shows a reasonably smooth film surface similar to the surfaces of all other films examined in this study.

Five similar NbN films were analyzed at Surface Science Western at the University of Western Ontario in London, Ontario. X-ray photoelectron spectroscopy (XPS) was performed using an SSX-100 (Surface Science Laboratories, California) spectrometer with a monochromatized Al $K\alpha$ X-ray beam focused either to a 300 or 600 μm spot size. Depth profiling was carried out with a 4 kV Ar^+ ion beam rastered over

a 2 mm x 2 mm area to give an equivalent sputter rate for SiO_2 of 100 Å/min. It was revealed with this study that our films contain several atomic percent of oxygen. While this is a significant impurity content it is not unusual for sputtered NbN films [10]. Furthermore, oxygen impurities of this magnitude are typical of nitrides of many metals such as titanium [11,12], tantalum [13], hafnium [11], zirconium [12] and niobium [14]. XRD work on other NbN samples grown under similar conditions does not reveal oxide phases of Nb (i.e. Nb_2O_5), hence we believe the oxygen to be adsorbed on grain boundaries [4] and incorporated largely after deposition.

Spectrophotometry measurement of film reflection was performed to confirm our spectroellipsometry results. Figure shows the measured reflection of sample F2, and is compared to values calculated using standard optical formulae from the spectroellipsometric dielectric constants. The good agreement from 1.5 to 4.0 eV suggests that the ambient substrate model used in the determination of the pseudo-dielectric function is reasonable, and that surface roughness is not significant. Other research [3] has shown that the highest T_c films are near-stoichiometric. We consider the pseudo-dielectric function of sample F2 to be most representative of NbN, since this sample had the highest critical temperature, T_c. Samples F4 and F6 are likely to have a metal excess (lower N_2 flow) whereas sample F0 is probably super-stoichiometric (higher N_2 flow).

Jillie et. al. previously reported that their films exhibiting strong NbN (111) and NbN (200) peaks yielded poor tunnel junctions if the T_c was below 15 K and they had low reflectivity in the UV-visible spectral region [15]. They presented empirical evidence of a correlation between film reflectivity and NbN electrode quality. In this study, all the films have a T_c below 15 K and are lower in reflectivity than the limit Jillie specified. We are currently experimenting with means of increasing film T_c and will try to verify this correlation between device quality and reflectivity. As the nitrogen flow decreased, we observed an increase in the reflectivity of the films. This trend is consistent through the operating point where our highest T_c film was deposited. Thus, we observe that NbN has a higher reflectivity than NbN_{1+x}.

Tanabe et. al. [3] reported that their optical constants n and k at energy 2.0 eV ranged from n = 1.6 to 1.8 and k = 2.6 to 2.9 for nearly stoichiometric films of high T_c deposited at ambient temperatures. At the same energy, our highest T_c film, F2, had n and k values of 1.6 and 2.1 respectively, showing reasonable agreement for n but a lower absorption in our films.

Motulevich et. al. [1] reported fine structure in the real part of the dielectric constant near 1.5 eV which they attributed to interband transitions. We do not observe any fine structure in our data, evidenced by Fig. 1. However, apart from this absence of fine structure, our results for the region 2.0 to 3.1 eV confirm those of Motulevich very well. For instance, at 2.5 eV we have ε_1 = -0.80 and ε_2 = 4.7 for sample F2, versus values of ε_1 = -0.6 and ε_2 = 4.3 for Motulevich.

Tanabe et. al. [3] used the Drude theory to obtain a three parameter fit to reflection spectra only, in the energy range 0.5 to 5 eV. Values of the high frequency lattice dielectric constant, ε_∞ varied considerably (12.5 to 17) between films. It is likely that there is a strong dependence of ε_∞ and other parameters on both stoichiometry and deposition conditions. To compare our results to others, an attempt was made to fit the measured dielectric function of our films to the Drude theory of free electrons [16]. A two parameter fit of the reciprocal relaxation time, γ, and the high frequency dielectric constant , ε_∞ , was performed. The best fit was obtained with ε_∞ = 5.0 and γ = 2.9 eV, using the plasma frequency ω_p = 2.98 eV, determined where $\langle\varepsilon_1\rangle = 0$. However the theoretical fit to the measured dielectric function was very poor, particularly for energies greater than 3.5 eV. We conclude that simple the Drude model is inadequate for NbN, which is not surprising based on the invalidity of the theory at high frequencies $\omega > \omega_p$ [17].

6. Conclusions

The pseudo-dielectric function of reactively sputtered NbN thin films was determined by spectroellipsometry over the energy range 1.5 to 5.0 eV, and confirmed

by spectrophotometry measurement of reflectance. The sample most representative of stoichiometric NbN was deposited at a nitrogen flow rate of 4.4 sccm. Drude free electron theory was found to be inadequate to explain the measured optical behavior, particularly at high energies.

Acknowledgments

The authors would like to thank R. Schmaus for his assistance in measurement of the T_c of the films. This research was supported by the Natural Sciences and Engineering Research Council of Canada, the Alberta Microelectronic Centre and the James Clerk Maxwell Telescope Instrument Development Fund.

References

1. G. P. Motulevich and N. D. Kuz'michev, Sov. Phys. JETP **57**, (1983) 1351.
2. G. P. Motulevich and N. D. Kuz'michev, Sov. Phys. Solid State **27**, (1985) 1583 .
3. K. Tanabe, H. As no, Y. Katoh, and O. Michikami, J. Appl. Phys. **63**, (1987)1733.
4. J.F.Vaneldik , K.L. Westra, D. Routledge and M.J. Brett , J. Phys. D. **22,** (1987) 1788.
5. K. L. Westra, R.P.W. Lawson, and M.J. Brett, J. Vac. Sci. Technol. A 6, (1988) 1730.
6. B.T. Sullivan and R.R. Parsons, J. Vac. Sci. Technol. A **5,** (1987) 3400.
7. K.L. Westra , M.J. Brett, and J.F. Vaneldik, J. Vac. Sci. Technol. A **8,** (1990) 1293.
8. J.A. Thornton Annu. Rev. Mater Sci. **7,** (1977) 239.
9. J.A. Thornton, J. Vac. Sci. Tech . A 4, (1986) 3059 .
10. M.J. Deen, Thin Solid Films **152,** (1987) 535 .
11. D.S. Yee, J.J. Cuomo, M.A. Frisch, and D.P. Smith, J. Vac. Sci. Technol. A **4**, (1986) 381 .
12. D.S. Williams, F.A. Baiocchi , R.C. Bearisto, J.M. Brown, R.V. Knoell , and S.P. Murarka, J. Vac. Sci. Technol. B **5**, (1987) 1732 .
13. P Mehotra . J. Stimmel , J. Vac. Sci. Technol. B **5**, (1987) 1736 .
14. L.C. Zhang, C.L. Liang, S.K. Cheung, and N.W. Cheung, J. Vac. Sci. Technol. B **5**, (1987) 1723 .
15. J. D. Jillie, H. Kroger, L. N. Smith, E. J. Caukasuskas, and M. Nisenoff, Appl. Phys. Lett. **40**, (1982) 749.
16. C. G. Granqvist and I. Hamberg, J. Appl. Phys. **60,** (1986) R137.
17. W. Dumke, Phys. Rev. **124**, (1961) 1813 .

Table 1. Properties of sputtered NbN films

Sample	N_2 flow (sccm)	ρ ($\mu\Omega$-cm)	Thickness (kÅ)	T_c
F0	4.7	394	9.28	12.9
F2	4.4	395	9.81	14.4
F4	4.3	292	11.42	13.9
F6	4.1	226	11.02	13.0

Figure Captions

FIG. 1. The pseudo-dielectric function $<\varepsilon_1>$ (bottom curve) and $<\varepsilon_2>$ (top curve) determined by spectroscopic ellipsometry. Solid line: sample F0, long dash: sample F2, short dash: sample F4, dot-dash: sample F6.

FIG. 2. SEM photograph of sample F4, showing structure typical of all samples studied.

FIG. 3. Optical reflectivity spectra of the highest T_c film studied, sample F2. The open circles represent values measured using a spectrophotometer. The light rectangles are reflectivity calculated from the permittivity data obtained from the ellipsometer study.

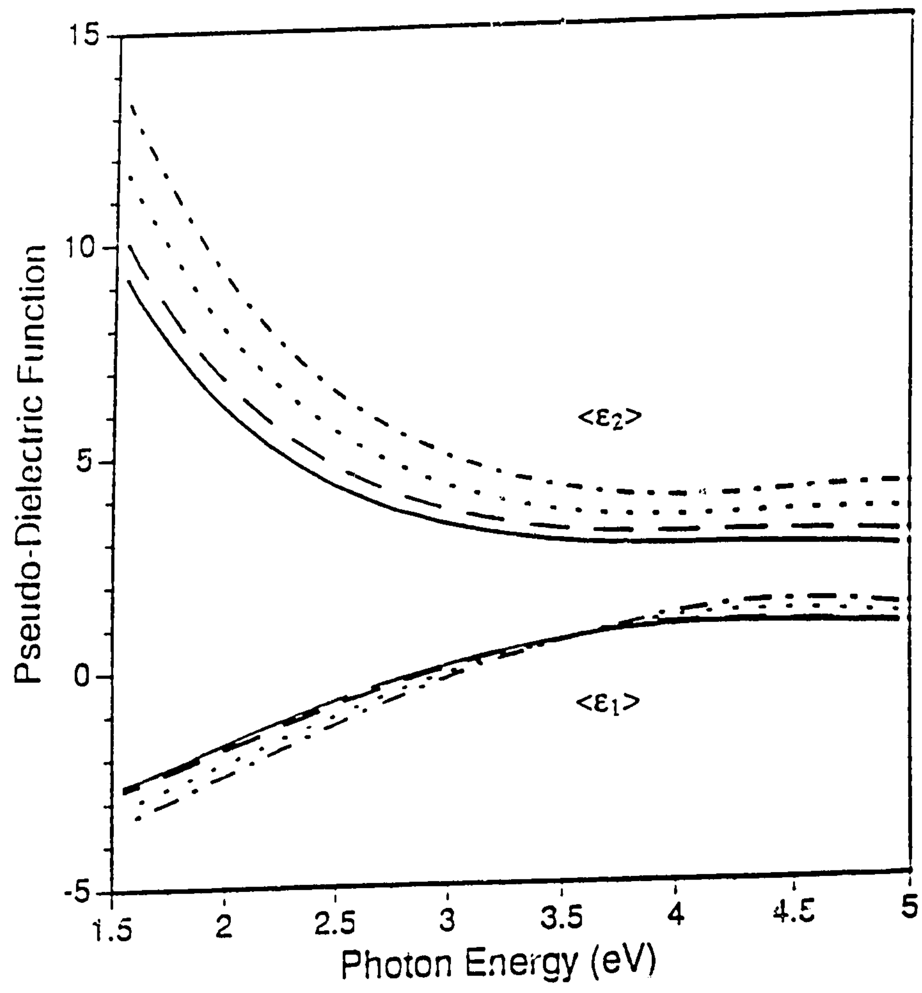

Pseudo-Dielectric Function
Photon Energy (eV)
<ε2>
<ε1>
15
10
5
0
-5
1.5
2
2.5
3
3.5
4
4.5
5

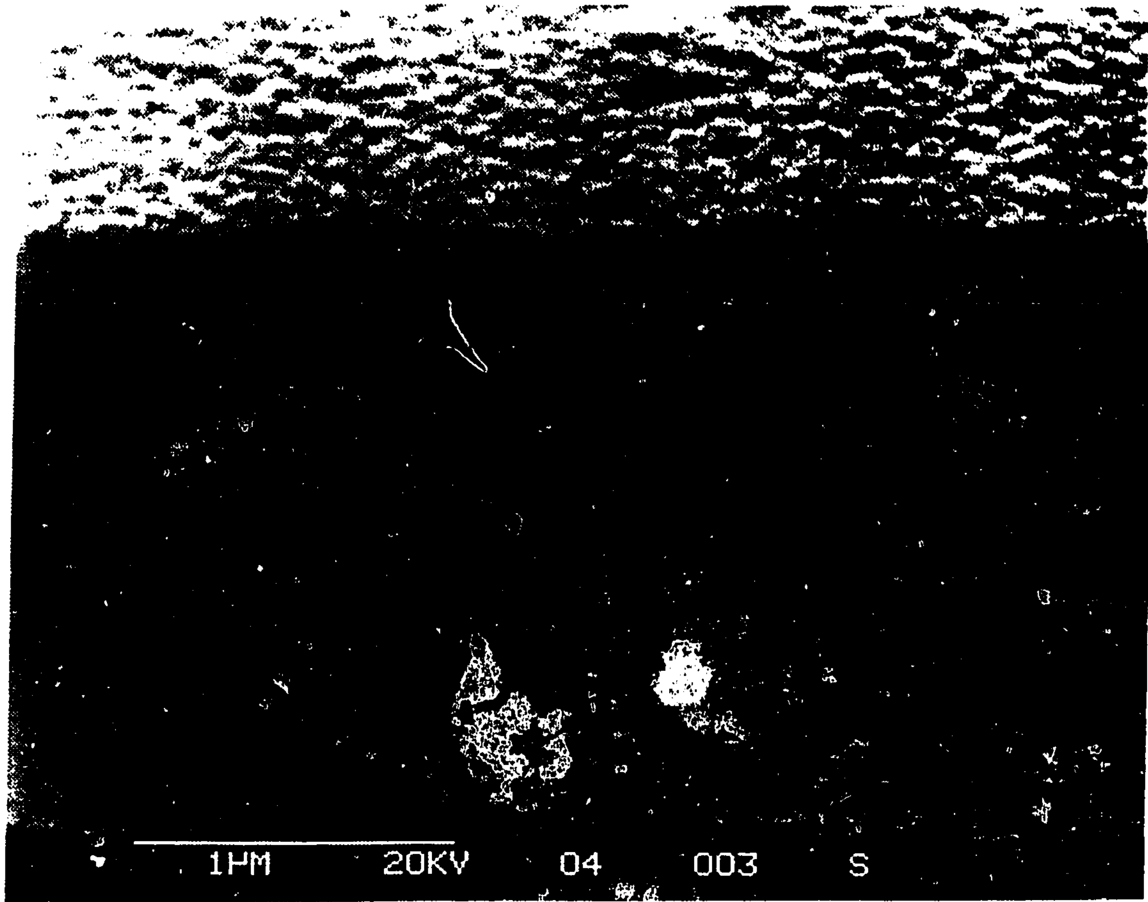
1PM
20KV
04
003
S

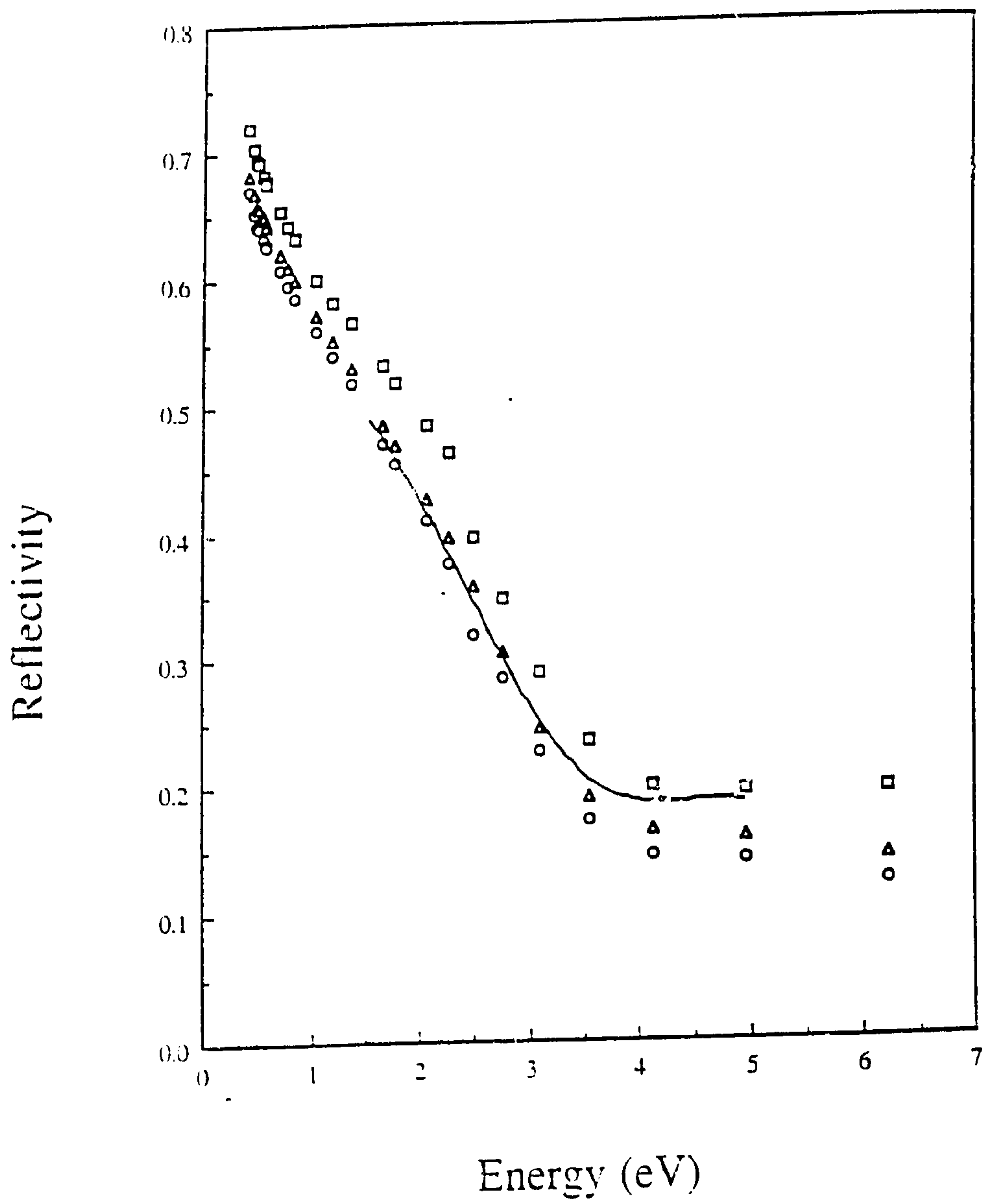
Reflectivity
0.8
0.7
0.6
0.5
0.4
0.3
0.2
0.1
0.0
0
1
2
3
4
5
6
7
Energy (eV)